Thesis for the degree of Doctor of Philosophy

OVERSTRETCHING SHORT DNA

SINGLE-MOLECULE FORCE SPECTROSCOPY STUDIES

NIKLAS BOSAEUS

Department of Chemical and Biological Engineering
Chalmers University of Technology
Gothenburg, Sweden 2013

Cover:
Schematic representation of the three overstretched states of DNA.

OVERSTRETCHING SHORT DNA

SINGLE-MOLECULE FORCE SPECTROSCOPY STUDIES

Niklas Bosaeus

Department of Chemical and Biological Engineering
Chalmers University of Technology

Abstract

Structural deformation of DNA has a central role in many biological processes. It occurs, for example, during replication, transcription, and regulation of the activity of the genome. To understand these fundamental processes it is necessary to have a detailed knowledge of the mechanical properties of DNA. How DNA responds to longitudinal stress has been studied on the single-molecule level for over two decades. Early it was discovered that torsionally relaxed double-stranded (ds) DNA undergoes a structural transition when subjected to forces of about 60-70 pN. During this overstretching transition the contour length of the DNA increases by up to 70% without complete strand dissociation. Since its discovery, a debate has arisen as to whether the DNA molecule adopts a new form or denatures under the applied tension. In the work of this thesis the overstretching transition is studied using optical tweezers to extend individual dsDNA molecules of 60 – 122 base pairs. By stretching short designed molecules of variable base-composition and with structural modification, factors determining the outcome of the process could be isolated and investigated. The structural changes induced during the transition vary depending on the stability of the dsDNA. Sequences that have a high GC-content are demonstrated to undergo a reversible overstretching transition into a longer form that remains base-paired. At high salt concentrations, this form of DNA, referred to as S-form, is found to be stable for extended periods of time, while at low salt it quickly denatures. AT-rich sequences are found to denature under tension in two different ways: if the AT-rich domain has one free end, melting will occur by progressive peeling of one strand from the other. When peeling is inhibited, here using synthetic inter-strand crosslinks, melting instead occurs internally within the sequence. The results presented here refine our knowledge of DNA mechanics, essential for understanding how proteins in our cells interact with DNA.

Keywords: DNA stretching, DNA structure, mechanical properties of DNA, single molecule, optical tweezers

List of publications

This thesis is based on the work contained in the following papers:

I   Niklas Bosaeus, Afaf H. El-Sagheer, Tom Brown, Steven B. Smith, Björn Åkerman, Carlos Bustamante, and Bengt Nordén
Tension induces a base-paired overstretched DNA conformation
Proceedings of the National Academy of Sciences, 2012, 109, 15179-15184.

II   Niklas Bosaeus, Afaf H. El-Sagheer, Tom Brown, Björn Åkerman, and Bengt Nordén
Force-induced melting of DNA - Evidence for peeling and internal melting from force spectra on short synthetic duplex sequences
Manuscript.

Contribution report

Paper I: Initiated project together with S.B.S. Performed and analyzed the experiments. Main author of the paper.

Paper II: Designed, performed, and analyzed the experiments. Main author of the paper.

Table of contents

1 Introduction

Knowing the properties of biological molecules is essential for understanding how a cell functions and interacts with its surroundings. The perhaps most well-known biological molecule is DNA, which given its central role in all organisms is also likely the most studied one. Many of the proteins that interact with DNA in the cell stretch, bend, twist or deform the molecule in various ways. Examples include the packaging of DNA into chromosomes, which involves tight wrapping around histone protein aggregates, and the DNA interaction with proteins involved in homologous recombination, the latter known to significantly extend the DNA during the process [1-3]. To fully comprehend these essential interactions, it is crucial to understand the mechanical characteristics of DNA.

Technological advances over the last three decades have made it possible to directly study individual molecules. The main advantage compared to bulk measurements is that singular (potentially uncommon) events and structural changes in the molecule can be studied. In bulk measurements, by contrast, any observed property is an average over the dynamic behavior of many molecules. This can be advantageous in some cases, as it may provide higher measuring sensitivity, but it can also mask the actual behavior of the molecules, which may have important implications for the biological processes mentioned above. To study dynamics in an ensemble of molecules requires synchronization of the population, so that changes evolve in unison over time. Achieving a coherent ensemble can in itself be a formidable task, and maintaining it over time even more so as random interactions with the surroundings introduce fluctuations that deteriorate the coordination between molecules [4]. By instead observing the dynamics of many molecules individually, these issues can be avoided and the characteristics of the population can be obtained.

Many of the developed single-molecule techniques allow manipulation of the molecule so that individual molecules can be moved around and directed forces can be applied to them. One such technique is optical tweezers which is the main experimental tool used in this thesis. In an optical tweezers set-up, light is used to trap and exert defined forces on refractive objects. These forces can be used to affect the dynamics, investigate the mechanical properties, or induce conformational changes in a molecule tethered to the trapped refractive object. The application of force to single DNA molecules has revealed a phenomenon known as the DNA overstretching transition: a DNA molecule that is stretched by its two ends will first

start to straighten as the two ends are moved apart. When the DNA is close to fully extended it gets increasingly harder to stretch any further, until it suddenly yields and becomes almost two times as long over a narrow force interval. Since its discovery, the nature of this structural transition has been a topic of debate. Does the DNA molecule adopt a new longer form or does it denature under the applied tension? In the work presented here the overstretching phenomenon has been studied in short, designed sequences of DNA. This strategy has allowed for systematic studies of how intrinsic properties (sequence, duplex stability) as well as external factors (ionic strength) govern the overstretching transition. The results presented here extend our knowledge regarding the nature of the transition and provide new insights that resolve a few of the issues that have been the source of the debate.

The thesis is organized in the following way: Chapter 2 introduces optical tweezers, the physical principle behind it and how they can be used to apply and measure forces on a single DNA molecule. The chapter also provides a description of how the optical tweezers instrument that has been used in the works of this thesis operates. Finally, chapter 2 outlines the procedure for performing stretching experiments on DNA.

Chapter 3 discusses DNA and its mechanical properties. Starting with a description of the structure of the molecule, the chapter then proceeds to introduce models used to describe the relation between extension of polymers and the applied stretching force. This is followed by a discussion of how the polyelectrolyte nature of DNA affects the mechanical properties of the molecule. Section 3.4 describes how the field of DNA stretching has evolved and how overstretching of DNA has been studied. The last section of the chapter gives a brief overview of gel electrophoresis and chemical processes that have been utilized to modify and characterize the structure of the DNA in this thesis.

Chapter 4 provides a summary of the performed experimental work and how it has been analyzed. The acquired results are also presented and discussed. In Chapter 5 concluding remarks regarding the work are given together with suggestions for future experiments.

2 Force-measuring optical tweezers

The work presented in this thesis is based on experiments where optical tweezers are used to indirectly apply force to single DNA molecules. In this chapter the physics behind optical tweezers will be explained. A description of the instrument used to perform the experiments will also be provided.

As the name implies, optical tweezers is a technique where light is used to manipulate small objects. In 1873 James Clerk Maxwell postulated that electromagnetic radiation, i.e. light, can exert pressure on matter. The forces that are generated when light collides with an object are relatively weak; we for instance are not knocked over when we open the blinds to let the morning light in. If we fall, the cause is to be found elsewhere, as even a focused spot of milliwatts of power only produce forces measured in units of piconewtons (10^{-12} N). The effect of radiation pressure can, however, be significant for microscopic objects since forces of that magnitude are generated in many biological and chemical processes.

In 1970, Arthur Ashkin published results from a series of experiments where the light from a focused laser beam was directed onto micrometer sized particles suspended in water [5]. The experiments showed that particles of materials with high indices of refraction, such as polystyrene, were drawn into the beam and accelerated in the propagation direction of the light. When the particles reached the end of the chamber they became trapped against the wall until the laser was turned off. Particles with a refractive index lower than that of the surrounding water - Ashkin used air bubbles - were instead repelled by the beam. By introducing a second beam directly opposite to the first, Ashkin was able to balance the acceleration of the refractive particles and trap them transiently within the solution. By 1986, Ashkin and his coworkers had improved the technique and could show that, under the right conditions, a stable trap was formed with just one highly focused beam [6, 7]. This type of setup allows three-dimensional trapping of particles varying in size from nanometers up to tens of micrometers at room temperature [8].

The ultimate aim of the optical trapping experiments was to catch and hold atoms. This turned out to be possible if the atoms were cooled to very low (10^{-3} K) temperatures before being injected into the trap. For the work in this field, one of Ashkin's coworkers, Steven Chu received the Nobel Prize in physics in 1997 [9-11]. Ashkin and coworkers also discovered that biological samples such as viruses, yeast cells, bacteria and organelles within cells could be trapped and manipulated [12-14]. Other early adopters of the technique proved that optical tweezers could be used to

measure the mechanical forces generated by the flagella of bacteria and sperm as they swim in solution [15, 16].

Optical tweezers can be used to study the mechanical properties of even smaller objects, such as macromolecules, by attaching them to micrometer-sized beads of for example polystyrene or silica. By trapping the beads in the optical trap, the macromolecules can then be manipulated indirectly by the force applied to the beads. For example, the DNA stretching experiments presented in this thesis are performed by attaching the ends of a single DNA molecule to two polystyrene beads. One of the beads is held stationary at the orifice of a micropipette within the fluidics chamber, while the other is held and manipulated by the optical trap. By moving the trapped bead away from the stationary bead the DNA molecule can be extended.

2.1   The physics behind optical trapping

The experiments performed by Ashkin and his coworkers illustrate that the forces acting on the trapped particles due to the radiation pressure can be divided into two parts: a scattering force, F_S pushing the particle along the beam axis, and a gradient force, F_G that pulls the particle toward the most intense region of the beam. The physics behind these force contributions can be described in two ways depending on the size of the trapped object. If the diameter of the object, d, is much smaller than the wavelength, λ, of the trapping light $(d \ll \lambda)$ we find ourselves in the Rayleigh regime and the object can be treated electrostatically as a point dipole. For particles with a refractive index n_p in a medium of refractive index n_m the scattering force in the direction of the incident beam of intensity I_0 is [7]

$$F_S = \frac{I_0}{c} \sigma_s n_m. \tag{1}$$

Here, c is the speed of light in vacuum and σ_s is the scattering cross section of the particle which depends on d, λ, and the ratio between the refractive indices of the particle and the medium (n_p/n_m).

The gradient force is a result of spatial intensity variations within a non-uniform beam which will attract the particle toward the most intense region. Optical traps are typically formed by using laser beams that have a Gaussian intensity distribution where the highest intensities are found in the center of the beam. The force in the direction of the intensity gradient can, in the Rayleigh regime, be described by

$$F_G = \frac{\alpha}{2} \nabla E^2, \tag{2}$$

where E, is the electric field of the light and α is the polarizability of the particle which is proportional to the volume of the particle and (n_p/n_m). The equations show that the forces holding the particle in the trap are proportional to the intensity of the light, particle size, and the ratio between the refractive indices.

When the size of the object is much larger than the wavelength of the light $(d \gg \lambda)$, the trapping force can be understood in terms of the reflection and refraction of the incident light by the particle. As photons have a momentum,

$$\vec{P} = \frac{h}{2\pi} \vec{k}, \qquad P = \frac{h}{\lambda} \tag{3}$$

where h is Plank's constant and $\vec{k}$ the wave vector, the particle will receive an impulse that is opposite and equal to the change in the momentum of the deflected light $\Delta\vec{P} = \vec{P}_{out} - \vec{P}_{in}$, in accordance with Newton's third law. If the refractive index of the particle is larger than that of the medium, a spherical particle will act as a positive lens and refract a photon hitting it near its edge by an angle θ toward the center of the particle (see Figure 1).
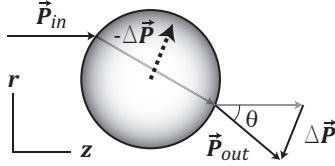
Figure 1 – Photons that are refracted an angle θ by a particle will change their momentum $\Delta\vec{P}$, and the particle feels an equal reaction impulse in the opposite direction $-\Delta\vec{P}$.

Since the total momentum always is conserved, this means that the particle will experience a force $\vec{F} = -d\Delta\vec{P}/dt$ in the opposite direction and move toward the original path of the photon. The same type of analysis can be extended to continuous rays of light, and allows us to examine cases where the intensity of the beam varies in space. A ray of light instead carries a linear momentum flux of magnitude

$$\left|\frac{d\vec{P}}{dt}\right| = \frac{n_m W}{c} \tag{4}$$

where W is the power of the ray. The resulting force on the bead can then again be related to the change in momentum of the refracted ray and expressed in its axial components, perpendicular to (r) and along (z) the beam as

$$F_r = \frac{n_m W}{c} \sin \theta$$
$$F_z = \frac{n_m W}{c} (1 - \cos \theta)$$

(5)

In Figure 2 the same particle is placed in a collimated beam with a Gaussian intensity distribution. The light impinging on the particle closer to the beam axis $\vec{P}_2$ is more intense than that of $\vec{P}_1$ and the net impulse received by the particle $-\Delta\vec{P} = -(\vec{P}_1 + \vec{P}_2)$ pushes it forward along the beam axis (z) but also inward toward the center of the beam. The contributions along the z- and r-directions in Figure 2 correspond to the scattering and gradient forces of equations 1 and 2, respectively. Once the particle reaches the center of the beam the forces in the r-direction will reach a stable equilibrium and the particle will only be propelled forward in the z-direction by the scattering force.
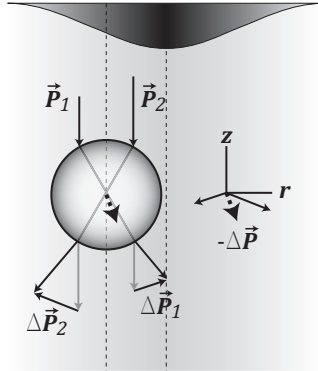
Figure 2 – Refraction by a particle in a collimated beam with a non-uniform intensity distribution. The resulting net force pushes the particle along the beam axis and up the intensity gradient toward the highest intensities.

To trap the particle in the z-direction the scattering force has to be balanced by a gradient force in the opposite direction. To do so the beam must be focused so that an intensity gradient is created along the z-axis. A stable trap relies on having a large fraction of the incident light coming in from steep angles relative to the z-axis. This is achieved by focusing the beam using a high numerical aperture (NA) microscope objective. The numerical aperture is a measure of the largest incidence angle, ϕ_m, that can be produced by the lens and is given by

$$NA = n_i \sin \phi_m \qquad\qquad (6)$$

where n_i is the refractive index of the medium between the lens and the sample. Typically the medium is water-based and water immersion objectives are used so $n_i \approx n_m \approx 1.33$. Figure 3 illustrates two cases where a refractive bead is situated near the focal point of a focused beam. Before the focal point (a.) the bead experiences an increased net force pushing it forward along the z-axis. By focusing the beam the overall intensity is significantly increased close to the focal point, which leads to stronger forces acting on the bead. Focusing also gives a steeper gradient in the r-direction, so confinement in the direction perpendicular to the beam axis is also increased. In the second scenario (b.), the center of the bead is downstream of the focal point and due to a large fraction of the light hitting the bead at a steep angle, the gradient force overcomes the scattering force and the net contribution acting on the bead is directed opposite to the propagation of the light along the z-axis. The bead will quickly reach a stable equilibrium at a position in between the two presented scenarios where the average net force is zero in all directions. For a single beam trap this point will be just downstream of the focal point. In the vicinity of the equilibrium point, the optical trap behaves as a linear spring that generates forces on the bead that are proportional to the displacement of it from the center of the trap.

Lasers used for trapping in optical tweezers commonly have near-infrared (NIR) wavelengths [17], and popular choices are the Nd:YAG laser (λ = 1064 nm) and diode lasers in the range λ = 800 – 900 nm. The wavelength of the trapping source is
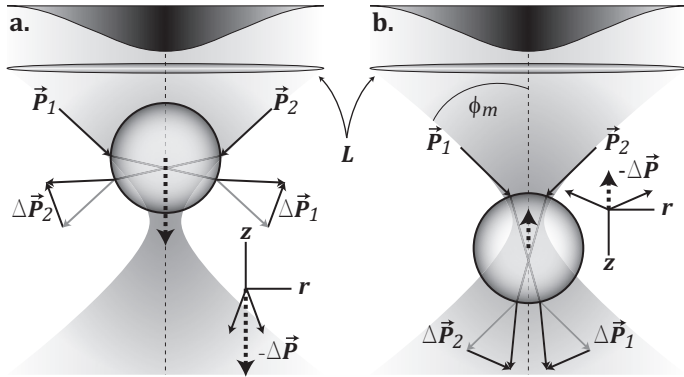

Figure 3 – A refractive bead located close to the focal point of a beam focused by a lens L (a.) At a position above the focal point the net reaction impulse due to the light impinging on the bead will push it away from the light source. (b.) Below the focal point the gradient forces overcome the scattering forces and the net impulse pulls the bead back toward the light source.

typically chosen as a compromise between laser availability and cost, and the relatively low absorption coefficient of water in this interval. Absorption of light leads to local heating of the medium around the trap, which influences the measurements and is difficult to compensate for. As the beads typically used in the experiments have diameters of one to a few micrometers, neither the Rayleigh $(d \ll \lambda)$ nor the ray optics $(d \gg \lambda)$ descriptions are strictly correct for NIR wavelengths. Theories do exist for the intermediate regime [8], however calculating the forces trapping the bead is generally not needed for operation of the trap since the forces can be measured.

While trapping a refractive particle in a focused laser beam is an exciting experiment, it is generally not the forces that are needed to do so that are of direct interest, but rather that they at equilibrium are opposite and equal to any other external force acting on the particle.

2.2 Measuring forces by light momentum

The optical tweezers instrument built and used during this thesis work measures the force by analyzing the angular intensity distribution of the light entering and leaving the trap. The method relies on collecting all the light rays that are refracted or reflected by the trapped bead to sum their contributions to the force. Collection of the light exiting the trap is done using a second objective lens opposite to the first. The light is collimated by the objective and passed onto photo-sensitive detectors where the change in the intensity distribution is measured. Figure 4 shows different scenarios where light entering from the top is focused by an objective lens and then refracted by a bead caught in the trap. The bead is shifted from its equilibrium position near the focal point by an external force, here represented by the dotted arrows, in a direction that is either transverse (r being in the x-y-plane) to (a. and b.) or along (c. and d.) the optical z-axis. For transverse forces, refraction by an angle θ_i will offset a ray i on the detector relative to its unperturbed zero-force trajectory by an amount [18]

$$\Delta r_i = r_{in} - r_{out} = R_L n_m \sin \theta_i \tag{7}$$

where R_L is the focal length of the objective lens. An external force applied to the bead along the optical axis expands the beam exiting the trap if it is directed toward the light source (c.) or narrows it if directed away from the source (d.).
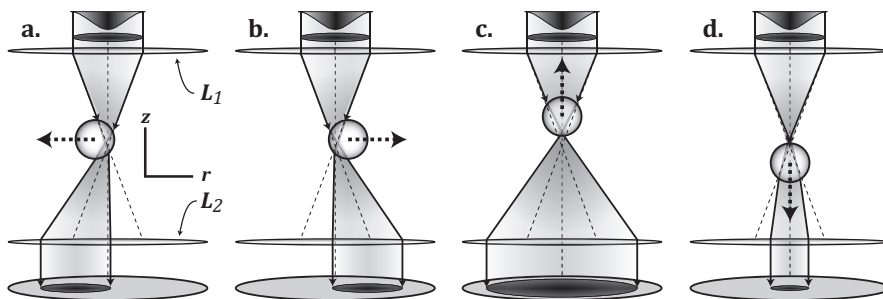
Figure 4 – Light, entering from the top, is focused by an objective lens (L_1) creating a trap that holds a bead. An external force applied to the bead (dotted arrow) shifts the equilibrium position of the bead within the trap. The light refracted through the bead is collected by a second objective (L_2) and passed on to a detector. (a.) A force applied to the left offsets light on the detector in the same direction. (b.) A force to the right reverses the offset. (c.) An axial force upward toward the light source expands the refracted beam while a force in the opposite direction (d.) narrows the cone of light.

Figure 4 also illustrates that if two identical objective lenses are used the back aperture of the focusing objective has to be under-filled, such that all of the deflected light fit within the numerical aperture of the collecting objective lens. However, under-filling the objective reduces the gradient forces and weakens the trap, so to form a stronger trap a second counter propagating light source is added to the system. Each light source gives a weak trap by itself but by focusing both to the same point one strong trap can be formed.

Figure 5 shows a schematic representation of the optical tweezers instrument used. The output from the two 150 mW, 845-nm diode lasers are guided through single-mode optical fibers to "fiber wigglers", which are devices that control the position of the formed trap in the plane (x, y) perpendicular to the optical axis (z) [19]. In the wigglers the optical fiber is passed through a set of brass tubes and comes out in the other end through a fine grid. The grid acts a pivoting point for the protruding fiber, and the angle in which the fiber is pointed in is controlled by piezoelectric actuators pushing on the brass tubing. The cone of light that emanates from the tip of the fiber is passed through a nitrocellulose pellicle beam splitter that redirects about 5% of the intensity onto a position-sensitive detector (PSD) where the x-y position is recorded.
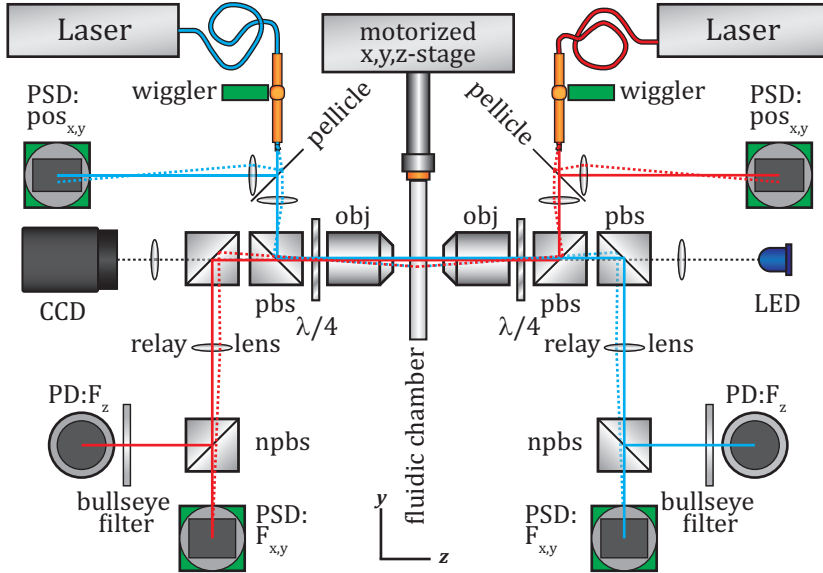
Figure 5 – Schematic representation of the optical tweezers instrument used in this thesis.

The remaining light is collimated by a lens, then redirected by a polarizing beam splitter (pbs) and passed through a quarter-wave plate ($\lambda/4$) before being focused through a water-immersion objective (obj, 60x, NA 1.20) to form the optical trap in the fluidic chamber. The quarter-wave plate transforms the linearly polarized light into circularly polarized light, thereby making the electric field homogenous in the plane perpendicular to the propagation direction of the light, and thus F_r cylindrically symmetric. The chamber is mounted to a x-y-z-microscope stage which can be translated using actuator motors. Both the stage and the wigglers are used to move the trap relative to objects in the fluidic chamber; large scale movements up to a few mm are performed by moving the stage, while movements on a nanometer scale are handled by the more precise wigglers. The wigglers only have a reach of about 10 μm from the center of the field of view in the transverse plane, so both systems are needed to position the trap in the chamber.

The light exiting the trap is collected by an identical objective lens and passed through a second quarter-wave plate. The quarter-wave plates turn the polarization of the light by 45°, which means that the light exiting the second plate has a polarization that is perpendicular relative to its original linear polarization. This allows the optical paths of the two lasers to be separated and the exiting light to be redirected for detection. After redirection by a second polarizing beam splitter, the light is passed

through a relay lens and divided using a non-polarizing beam splitter to divert light to both a PSD and a photodiode (PD) for force measurement in the x-y plane and along the z-axis, respectively. The purpose of the relay lens is to reimage the back-focal-plane of the objective lens onto the force detectors. Before the light hits the photodiode it is passed through a graduated "bullseye" filter to radially attenuate the beam so that the force signal along the z-axis can be scored properly. One of the objective lenses is mounted on a linear stage which allows positioning of it along the z-axis to focus the two beams in the same plane. The experiment is monitored using a CCD camera mounted on the optical axis. The illumination is provided by a LED emitting blue light, which is unaffected by the polarizing optics which are selected to match the wavelength of the lasers. The dotted red and blue lines illustrate the path of the light as the wigglers move the position of the trap in the chamber. The key point illustrated by the lines is that the position change is registered as an offset on the position-PSDs while the optical layout of the instrument ensures that the light hitting the force-PSDs is not displaced when the trap is moved.

The external forces applied to the trapped bead are obtained by summation over the spatial intensity distribution of all rays entering, $W(x,y)_{in}$ and exiting $W(x,y)_{out}$ the trap. These can be expressed as the distance weighted sums of the light intensities $\sum_i W_i x_i$ and $\sum_i W_i y_i$, which combined with equations 5 and 7 give the forces along the three axes as [20]

$$F_x = \frac{1}{R_L c}[(\sum_i W_i x_i)_{in} - (\sum_i W_i x_i)_{out}]$$
$$F_y = \frac{1}{R_L c}[(\sum_i W_i y_i)_{in} - (\sum_i W_i y_i)_{out}] \tag{8}$$
$$F_z = \frac{n_m}{c}\left[\left(\sum_i W_i \sqrt{1-(r_i/n_m R_L)^2}\right)_{in} - \left(\sum_i W_i \sqrt{1-(r_i/n_m R_L)^2}\right)_{out}\right]$$

When the trap is empty or when no external forces are applied to the trapped bead, the intensity sums of the light entering and leaving the trap are equal and the terms cancel. As the light entering the trap is unaffected by displacements of the bead in the trap by external forces, the detector signals measured in the absence of force can be used as a reference. This means that it is only necessary to measure the light exiting the trap, which gives a response relative to the zero-force reference.

The light hitting the photo-sensitive detectors give rise to a current that is proportional to the intensity of the light. The measured currents have to be calibrated in order to convert the signals into forces. Transverse forces are measured by PSDs where the signals in the two directions X and Y relative to the light intensities hitting the detector are given by

$$X = \frac{\Psi}{R_D}\sum_i W_i x_i$$
$$Y = \frac{\Psi}{R_D}\sum_i W_i y_i \tag{9}$$

where Ψ is the intensity response, and R_D the half-width or radius of the detector. Insertion of equation 9 into equation 8 gives

$$F_x = \frac{\Delta X R_D}{c\Psi R_L}$$
$$F_y = \frac{\Delta Y R_D}{c\Psi R_L} \tag{10}$$

where ΔX and ΔY are the detector signals relative to the zero-force references. Since the trap is formed by two laser beams that are detected independent from each other, the signals from the detectors along each axis are added to give the total force acting on the bead. The forces along the z-axis are detected by photodiodes that produce a signal proportional to the total intensity of the incoming light. However, as seen in Figure 4 (c. and d.) the total intensity hitting the detector does not vary with the displacement of the bead along the z-axis as long as all the light is collected. The problem is solved by introducing a "bullseye" filter directly in front of the photodiode which attenuates the light based on the size of the beam. The filter has a circular transmission profile $T \propto \sqrt{1 - (r/n_m R_L)^2}$, where r is the radial distance from the center. The equation shows that the filter profile has to be made to fit the focal length of the objective lens and a specific refractive index for the medium (typically that of pure water). The result is a signal Z from the detector that is proportional to the intensity distribution as

$$Z = \Psi_z \sum_i W_i\sqrt{1 - (r_i/n_m R_L)^2} \tag{11}$$

where Ψ_z is the responsivity of the diode. Using equation 8 and taking the difference between the relative signals of the two photodiode detectors ΔZ_A and ΔZ_B, the force acting along the z-axis can be calculated.

$$F_z = \frac{n_m}{c\Psi_z}(\Delta Z_A - \Delta Z_B) \tag{12}$$

Equation 10 shows that the calibration of the transverse forces only relies on constant physical parameters of the instrument itself which can be measured using a power meter, a ruler, and the detectors. This means that the calibration is

independent of the size, shape or refractive index of the beads, the viscosity and refractive index of the medium, and the laser power, which are all parameters that can change between or during experiments. The same applies to the z-force calibration except for the refractive index of the medium as seen in equation 12. At a 1 M concentration of NaCl the refractive index is about 1% higher than that of pure water, and F_z will have an error proportional to the change. The resulting error is however typically small (<0.25%) for weak forces [20].

Besides measuring the forces acting on the trapped bead, the instrument also records the position of the formed trap as it is moved by the wigglers. Calibration of the PSDs measuring the position is performed by tracking a bead that is fixed to the fluidic chamber using a feed-back protocol where the trap is moved to maintain a constant force. The chamber is then translated along the x- and y- axes by the actuator motors and the detector signal can then be calibrated using the known step size of the motors. The calibrated instrument allows a force resolution of about 0.1 pN and a position resolution of 0.5 nm. For polystyrene beads, with diameters of 2-3 μm in a water based medium, the formed trap can hold the beads up to forces of about 140 pN.

The described optical tweezers instrument does not directly measure the displacement Δx of the bead within the trap. In many other instrument setups, the displacement is measured instead of the force. The reason why this is an alternative approach is that there is a linear relationship between the force and small displacements given by Hooke's law for a spring,

$$F = \kappa \Delta x \qquad (13)$$

where κ is the stiffness or spring constant of the trap. Using other techniques, the displacement of the bead can be measured with very high resolution; back-focal-plane interferometry for instance is capable of tracking Ångström changes in the bead position on a submillisecond timescale [17]. If the position signal is calibrated, equation 13 leaves κ as the parameter that should be determined to connect the position of the bead to the force applied to the bead. Alternatively, if the force is measured as in the instrument used here, the relation can be used to calculate the displacement of the bead within the trap provided that κ is known.

As the described setup has two counter propagating lasers that can be independently positioned, the transverse stiffness of the trap can be measured by moving the lasers in opposite directions within a trapped bead. The two beams are moved until a small set change in the force is reached for each of the traps. Since the

traps are moved in opposite directions by distances equaling an identical force, the total force remains constant. The distance required to obtain the change in force is measured and the stiffness is then calculated using equation 13. The method allows the stiffness of the trap to be sampled at several different forces, which means that deviations from the Hookean behavior can be accounted for.

Figure 6 shows a plot where the force is recorded as a function of the trap position when the trap is moved across a bead that is held stationary on top of a pipette in the fluidic chamber. The S-shaped curve shows how moderate displacements of the trap relative to the center of the bead give an approximately linear force response. When the position of the trap approaches the radius of the bead the slope starts to deviate and reaches a maximum close to the edge, after which the force rapidly declines.
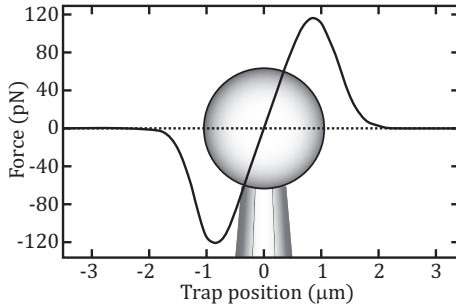

Figure 6 – Force vs. trap position plot of a 2 μm bead that has been immobilized by sucking it onto a pipette in the fluidic chamber. The trap is moved horizontally across the bead which generates an S-shaped force response along the same axis. The experiment illustrates the approximately linear relation between the force and moderate displacements of the bead within the trap.

An independent way of verifying the force calibration is to test it against a known force. The force can be an externally applied drag, generated by moving the medium surrounding the bead (or the other way around) at a known velocity v. The drag force is then determined using Stokes' law, which for a sphere of diameter d is

$$F = 3\pi\eta dv = \gamma v \tag{14}$$

The method relies on knowing the viscosity η of the medium, but also the exact size and shape of the bead so several beads of a known distribution have to be sampled. The tests are preferably performed away from the surfaces of the fluidic chamber as the drag coefficient γ of the bead increases close to a surface [8].

2.3   Performing optical tweezers experiments

The DNA stretching experiments in this thesis are performed by tethering the ends of a molecule to two refractive polystyrene beads. One end of the DNA is labelled with biotin (vitamin B_7), that binds strongly ($K_d \sim 10^{-15}$ M) to streptavidin

which is a protein purified from the bacteria *Streptomyces avidinii* [21]. The other end of the DNA is labelled with digoxigenin which binds to digoxigenin antibodies. The labelled DNA is typically incubated with polystyrene beads that have anti-digoxigenin cross-linked to the surface to bind one end of the DNA before introducing the beads to the fluidic chamber (see Figure 7b). The other, biotin labelled, end of the DNA is linked to a streptavidin-coated bead in the fluidic chamber. Figure 7 also shows the layout of the chambers used. The top and bottom of the chamber are made from two 24x60 mm #1.5 cover slips. In the top cover slip holes are cut using a laser engraver to form inlets and outlets for buffer and beads. Using the laser engraver, gaskets with three channels are made out of nescofilm. The two gaskets are then put on the cover slips and aligned with the inlet and outlet holes. A glass pipette and tubes connecting the top and bottom channels with the middle one are placed in between the gaskets. The pipette is pulled by threading a glass capillary tube through a coil of platinum wire, heating it by running a current through wire while at the same time applying a tension to the tube. The pipette is pulled so that the resulting tip has an orifice with a diameter of about one μm.
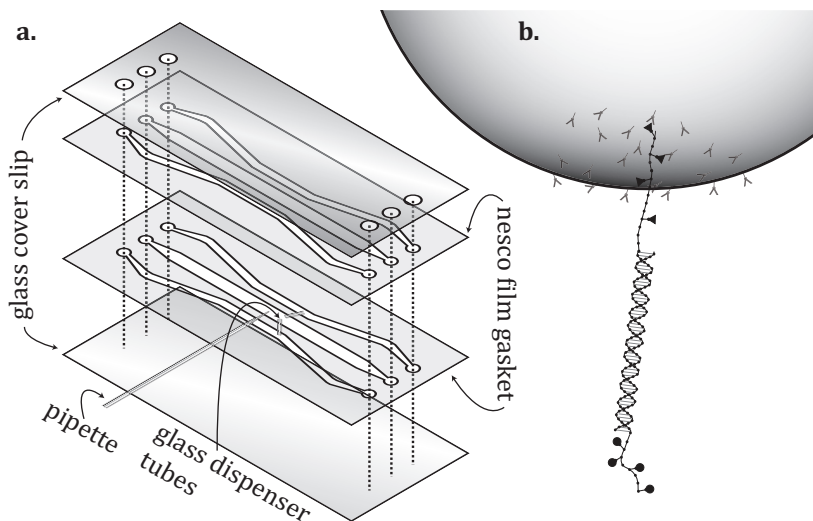
Figure 7 – (a.) A fluidic chamber is created by making a sandwich out of cover slips with gaskets made from nescofilm in between. Before sealing the chamber by heating it, a fine glass pipette and tubes that connect the three channels are placed between the gaskets. The finished chamber is placed in an aluminum holder that allows polyethylene tubing to be connected to the inlets and outlets of the chamber. The holder is attached to the x-y-z-stage of the instrument. (b.) DNA enters the chamber pre-attached to one of the two types of beads that are coated with either streptavidin or anti-digoxigenin.

Figure 8 – Assembling DNA and beads in the fluidic chamber. (a.) Overview of the fluidic chamber. The chamber has three channels with inlets and outlets for buffers and sample. The top and bottom channels are used to bring in the two different sets of coated beads together with the DNA sample. A pipette is placed so that the tip is located in the middle channel, where experiment is performed. Two dispenser tubes connect the top and bottom channels to the middle. (b.) First a streptavidin coated polystyrene bead is captured by moving the chamber so that the trap is close to the dispenser tube from which bead are being flowed. (c.) The captured bead is then moved and sucked out of the trap onto the pipette. (d.) Next, a second bead carrying the DNA is captured at the second dispenser tube. (e.) The bead is brought back to the pipette and the free biotin labelled end of the DNA is bound to the streptavidin bead on the pipette by bringing the two beads close to each other. The established tether is then tested to check that only one DNA molecule is connected between the beads. Stretching is then performed by moving the trapped bead away from the one on the pipette using the wigglers.

a. Fluidic chamber overview

b. Catch bead at dispenser tube

c. Move bead to pipette

d. Get bead with DNA

e. Connect DNA to bead on pipette
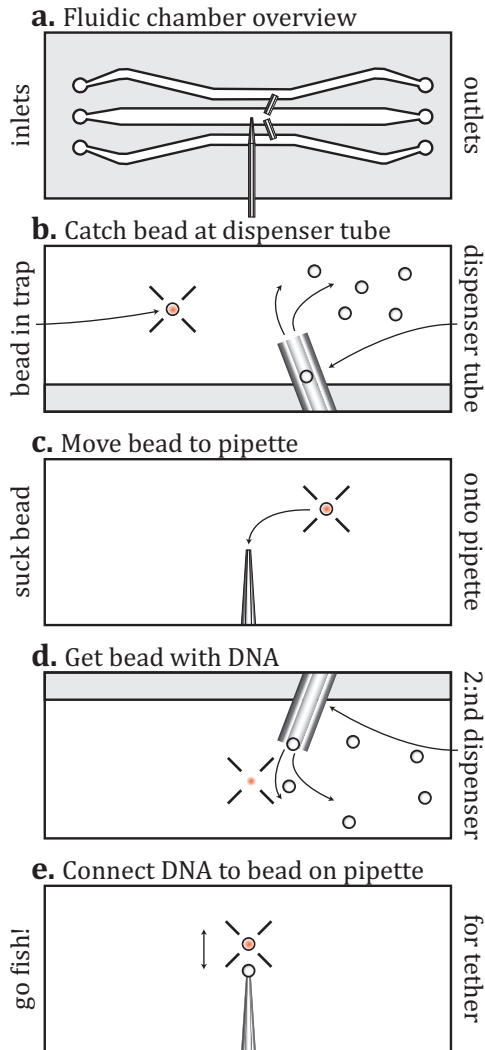
After placing the pipette and the dispenser tubes, the chamber "sandwich" is sealed by heating it to the melting point of the nescofilm. The purpose of the pipette is to immobilize one of the beads in the experiment, and this is done by sucking it on to the tip. The glass tubes connecting the channels are used to dispense the two types of beads that are brought in through the top and bottom channels. Figure 8 shows how the instrument is used together with the fluidic chamber to assemble the experiment. The DNA is suspended between the one bead held in the trap, and another that is fixed by sucking it on to the pipette. Once a tether has been established the DNA is stretched by moving the trap via the wigglers. By analyzing the resulting force response it can be ensured that it is only one molecule that bridges the two beads.

3   DNA

In this chapter the structure of DNA is introduced together with models describing how it is influenced by external forces. The chapter also addresses the DNA overstretching transition, which is the main phenomenon of study in this thesis. In the last part of the chapter methods that have been used to chemically modify DNA are presented.

3.1   The structure of DNA

DNA or 2'-deoxyribonucleic acid is one of the most well-known chemical substances, being the carrier of our hereditary information. Although DNA was first extracted from cells as early as 1869 by Friedrich Miescher, its biological importance was not immediately understood. Miescher himself thought that the role of DNA was nothing more than to store phosphor in the cell [22]. It would take almost a century of scientific efforts before the true role of DNA was revealed. In 1928 Frederick Griffith performed a series of experiments where he injected mice with different types of *pneumococcus* bacteria [23]. One type was virulent and caused the mice to develop pneumonia and die within a few days. If the same type of bacteria was destroyed by heating the sample before injection the mice survived the treatment. A second type of bacteria was by the same protocol shown to be harmless to the mice on its own, but when Griffith injected a mixture of the harmless and the heat-killed deadly type of bacteria, the mice soon developed pneumonia and died. When Griffith examined the bacteria from the deceased mice he found live cells of the virulent type, which suggested that a substance from one cell could genetically transform another cell. In 1944 Oswald Avery and coworkers showed that the substance in question was DNA [24]. While this discovery pushed DNA into the spotlight as the molecule responsible for carrying hereditary information, the question of how the information was stored in DNA and read by the cell was still a puzzle.

At the time of Avery's discovery, the chemical composition of DNA was fairly well known. Researchers knew that DNA is a polymer where the repetitive unit is a nucleotide, which consists of a pentose sugar with a heterocyclic base and a phosphate group. Figure 9 shows the chemical structure and numbering system of a nucleotide. The polymer is formed by connecting the phosphate group of one nucleotide to the sugar of another nucleotide, creating an alternating chain of sugar and phosphodiester groups. The polynucleotide chain has directionality, as the ribose sugar of a nucleotide is connected to the previous unit by
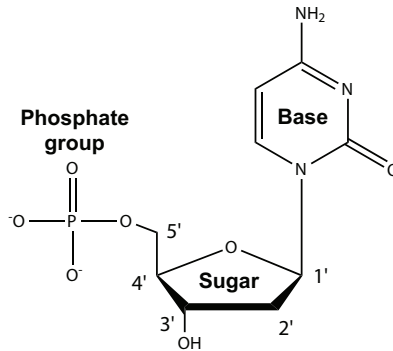
Figure 9 - A nucleotide consists of a phosphate group, a pentose sugar (2'-deoxy in DNA), and a base (here cytosine).

the 5'-carbon and the next through the 3'-carbon. By convention, the order of the nucleotides in a sequence is specified in the 5'-to-3' direction. At physiological pH the phosphodiester groups are monovalent anions, hence the 'acid' in ribonucleic acid: thus DNA is a polyanionic molecule where each phosphodiester group carries a negative charge. Figure 10 shows the four different bases that are found in natural DNA: adenine (A), cytosine (C), guanine (G), and thymine (T). The bases are of two types; adenine and guanine are purines, and cytosine and thymine are pyrimidines. Another piece to the genetic puzzle was added when Erwin Chargaff in 1951 discovered that there was a constant pattern in the amounts of each base in DNA extracted from several species. The amount of adenine was always equal to the amount of thymine, and the amount of guanine was always equal to the amount of cytosine [25].

The answer to the question of how the genetic information is encoded in DNA came with the discovery of the structure of the molecule. In 1953, James Watson and Francis Crick proposed that DNA was organized as an antiparallel double helix [26]. The suggested structure placed the charged phosphodiester backbones of the two intertwined DNA strands on the outside of the helix running in opposite directions. The bases were stacked like a roll of coins in the center, with adenines on one strand paired with thymines on the other and guanines paired with cytosines according to Chargaff's rule. Pairing a purine with a pyrimidine base ensures that the radius of the formed double helix is constant throughout the polymer, and is a prerequisite for the structural integrity of the same. In their paper Watson and Crick stated that "It has not escaped our notice that the specific pairing we have postulated immediately suggests a possible copying mechanism for the genetic material". The authors
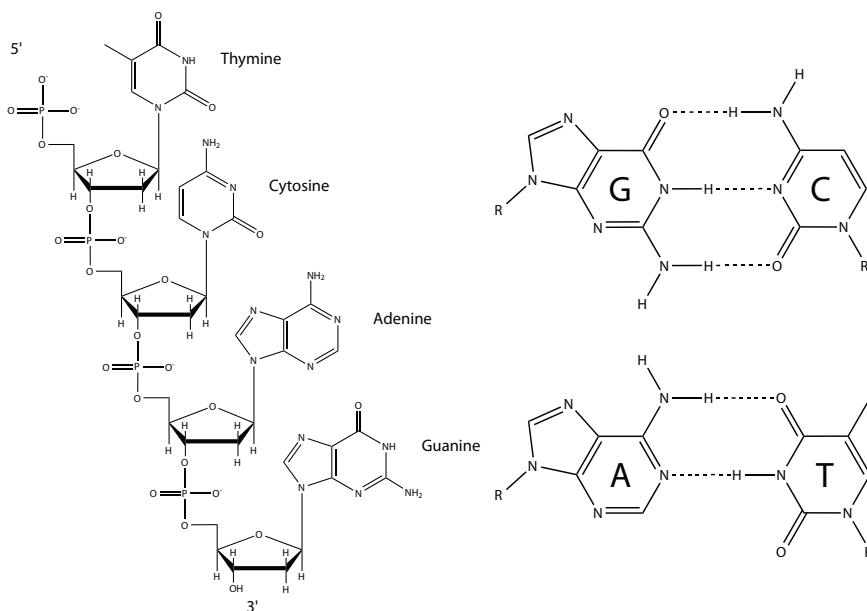
Figure 10 - (Left) The structure of single-stranded DNA with the four bases Thymine, Cytosine, Adenine, and Guanine. The nucleotides are linked together through phosphodiester bonds. (Right) The complementary bases pair by hydrogen bonding, A and T form two hydrogen bonds while G and C form three.

elaborated on the biological implications of their proposed structure in a follow up paper later the same year [27]. In the paper they argued that given the many possible base permutations in a long molecule, it is the precise sequence of the bases that carries the genetic information. Given the order of bases on one chain, the specific pairing rules allow determination of the exact order of the other one. This complementarity of the two strands, where each strand can act as a template for the other, was proposed to be the mechanism for replication of DNA.

The double helical configuration was based on X-ray diffraction data by Franklin and Wilkins [28, 29]. Their measurements of "structure B" had shown that the DNA likely was organized with two strands in a helical configuration, with an outer diameter of ~20 Å (1 Å=10^{-10} m) and a regular distance of 3.4 Å between the ten residues of a single turn repeat unit. This B-form is the main conformation of DNA under physiological conditions. The way the two strands are intertwined results in two grooves along the helix. One wide, called the major, and one narrow minor groove. These structural features provide access to the bases and are important in the interaction with many DNA binding molecules. In the B-form, each base pair (bp) lies flat almost perpendicular to the long axis of the helix forming two hydrogen

bonds in the A – T pair, and three in the G – C pair. The extra hydrogen bond[1] means that G – C base pairs are slightly more stable than A – T base pairs. This is observed in thermal melting experiments where the stability of the double-stranded DNA is determined; GC-rich DNA is generally melted into two single-strands at higher temperatures than AT-rich sequences.

The total number of hydrogen bonds between the two DNA strands is not the only factor that determines the stability of the helix; for a given length and number of A – T and G – C base pairs in the polymer, the order in which they are organized must also be taken into account. This is a result of variation in the hydrophobic stacking interactions between neighboring base pairs, such that a sequence with alternating guanines and cytosines (GCGCGC) is more stable than a sequence of the same length with several G:s or C:s in a row (GGGCCC) [30]. A third important factor is the repulsion between the charged phosphates of the backbone. The destabilizing effect of these interactions is affected by the concentration of positively charged cations in the buffer that screens the charges of the backbones from each other. The effect is that the net charge of the polymer is reduced in high salt concentrations stabilizing the duplex, while in low salt conditions the backbones are less screened and the repulsion is stronger which leads to a less stable double-helix.

If the water activity is reduced, the DNA can adopt a different conformation called A-form [31]. In this conformation the twist of the double-helix is slightly lower with 12 bases per turn instead of 10 in B-form. The rise per base is also different from B-form with an average of 2.9 Å instead of 3.4 Å, and the bases exhibit an inclination of about 20° from perpendicularity. A third distinct DNA conformation is the Z-form, named after the observed zigzag pattern of the backbones [32, 33]. The perhaps most notable feature of Z-form DNA is that it is a left-handed helix. Figure 11 show the structures of the three double-stranded conformations.

---

[1] In the original papers by Watson and Crick, G – C pairs only formed two hydrogen bonds.
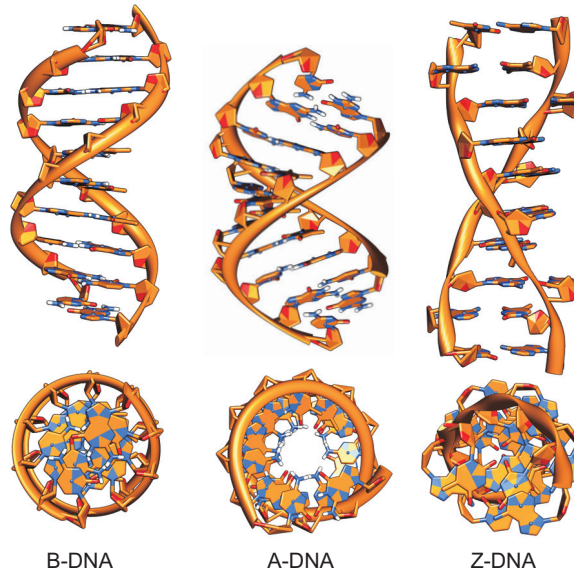
Figure 11 - The A-, B-, Z- of double-stranded DNA conformations. The A- and B-forms are right-handed helices, while the Z-form is left-handed. Under physiological conditions the DNA typically adopts the B-form. Adapted from ref. [34].

3.2   Modeling DNA as a polymer

In terms of a polymer DNA can be classified as a linear - i.e. it is generally not branched - heteropolymer with four different nucleotide monomers. Like other polymers it has a certain amount of flexibility, which means that a DNA molecule will rarely be perfectly straight. The constant bombardment of the surrounding solvent molecules, together with internal vibrations and rotations, introduces bends in the DNA polymer which over the length of the molecule can become significant. As many proteins in the cell interact with DNA by bending and stretching it, it is important to understand the mechanical properties of the DNA itself. Every nucleotide in a single DNA strand consists of 31-34 atoms, which means that in double-stranded DNA where the monomer usually is taken as a base pair, there are 65 or 66 atoms. Even if we consider only one DNA molecule, this single molecule can have thousands or hundreds of thousands of base pairs, with roughly the same amount of water molecules and counterions associated to it. To try to keep track of all atoms and their interactions with each other is a formidable task even for much smaller molecules, so a significant amount of abstraction is typically needed to characterize such a molecule. Luckily, even relatively simple polymer models can help

us understand and describe how DNA behaves in solution and under an external force. In this section two such models will be briefly presented.

3.2.1   The freely jointed chain

The simplest model describing a polymer conformation is the freely jointed chain (FJC). In the model the polymer is treated as a chain of identical rigid subunits connected by perfectly flexible hinges. Any interactions between the subunits are ignored, which means that steric interactions are neglected and the chain is allowed to intersect itself. Put in another way, the polymer is infinitely thin and has no volume, only N completely randomly oriented rigid segments of length b connecting $N + 1$ points in space. The polymer segments can thus be described by a series of vectors, $\vec{l}_i$, following each other from one end to the other (see Figure 12). The end-to-end vector connecting the two ends can then be calculated as the sum of all the link vectors.

$$\vec{r} = \sum_{i=1}^{N} \vec{l}_i \tag{15}$$

However, equation (15) does not provide much information, since for a randomly chosen conformation, $\vec{r}$ can point in any direction and have a length between zero and Nb. If we consider the ensemble average end-to-end vector we will find that it is $\langle \vec{r} \rangle = 0$, since the individual link vectors are uncorrelated and have no preferred spatial orientation (i.e. $\langle \vec{l}_i \cdot \vec{l}_j \rangle = 0$ for $i \neq j$). In this case a better estimate of the end-to-end distance is provided by the mean-square of $\vec{r}$,

$$\langle r^2 \rangle \equiv \langle \vec{r}^2 \rangle = \sum_{i=1}^{N} \sum_{j=1}^{N} \langle \vec{l}_i \cdot \vec{l}_j \rangle = \sum_{i=1}^{N} \langle \vec{l}_i^2 \rangle + 2 \sum_{i=1}^{N} \sum_{j=i+1}^{N} \langle \vec{l}_i \cdot \vec{l}_j \rangle$$

$$= Nb^2 + 2b^2 \sum_{i=1}^{N} \sum_{j=i+1}^{N} \langle \cos \theta_{ij} \rangle = Nb^2 \tag{16}$$

where θ_{ij} is defined in Figure 12. The lack of correlation between segments makes the calculation straightforward. The square root of the mean-square end-to-end distance gives us a value of the typical extension of the chain.
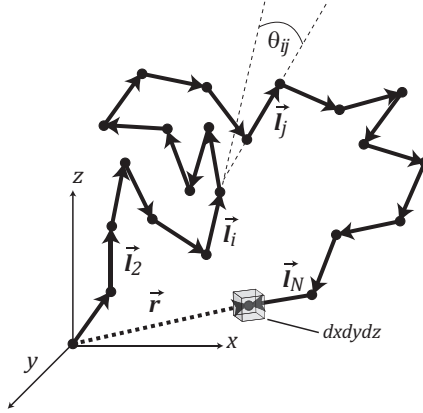
Figure 12 – The freely jointed chain model describes the polymer as series of N rigid segments of length b. The orientation of a segment, i, along the chain is represented by a vector $\vec{l}_i$.

$$\sqrt{\langle r^2 \rangle} = b\sqrt{N} \tag{17}$$

If these results seem familiar, it may be because they are analogous to a 3D random walk process with step size b. So how does this model relate to a real polymer? The assumption that the segments are freely jointed is quite crude, since a real polymer does come with restrictions for bending. The restrictions can be due to e.g. steric or electrostatic interactions between neighboring parts of the chain or certain preferred bond angles in the backbone of the polymer. Such constrains stiffen the chain as fewer conformations are possible relative to the case of free joints. The FJC model compensates for this by using a segment length, b, that typically is longer than the length of the monomers in the real polymer. The real restrictions in the polymer can thus be approximated by choosing fewer but longer segments when describing the chain. If we measure the mean-square end-to-end distance $\langle r^2 \rangle$ of a sufficiently long polymer of contour length L, we can then map the FJC model onto the real chain by choosing N and b as

$$\begin{aligned} Nb &= L \\ Nb^2 &= \langle r^2 \rangle \end{aligned} \tag{18}$$

The conditions above are satisfied by

$$N = \frac{L^2}{\langle r^2 \rangle}$$
$$b = \frac{\langle r^2 \rangle}{L} \qquad (19)$$

The segment length, b, is called the Kuhn length and describes the stiffness of the chain [35]. For a long freely jointed chain with one end at the origin, the probability of finding the other end of the chain in a volume element $dxdydz$ at $\vec{r}$ (see Figure 12) can be approximated by a Gaussian distribution [36]. We have already calculated the mean as $\langle \vec{r} \rangle$ (i.e. $= 0$) and the variance is given by

$$\sigma^2 = \langle \vec{r}^2 \rangle - \langle \vec{r} \rangle^2 = \langle r^2 \rangle - \langle 0 \rangle^2 = Nb^2 \qquad (20)$$

Then the probability distribution is,

$$p(\vec{r}) \equiv p(x, y, z) = \left(\frac{3}{2\pi Nb^2} \right)^{\frac{3}{2}} \exp\left(-\frac{3r^2}{2Nb^2} \right), \qquad (21)$$

where $r^2 = x^2 + y^2 + z^2$. If we do not care about the direction that the chain is extended in, we can multiply $p(\vec{r})$ by $4\pi r^2$ and get the radial distribution. The two distribution functions are plotted in Figure 13 for a case with $N = 100$, and $b = 1$ along with the root-mean-square length. Knowing $p(\vec{r})$, means that thermodynamic properties such as the entropy and the free energy of the chain can be calculated. The goal is to obtain an expression for the relation between an applied force and the end-to-end distance.
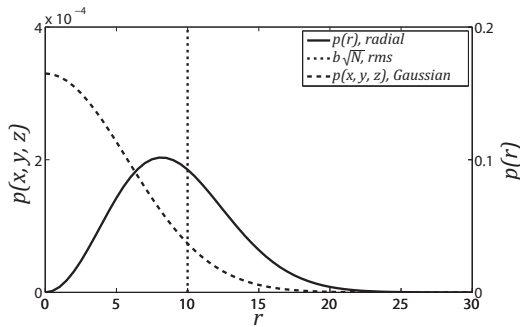

Figure 13 – Graph showing the approximative Gaussian distributions of the FJC end-to-end distance together with the expected rms-value for a chain with $N = 100$ and $b = 1$.

The number of conformations that the chain can assume between the two end points of the chain, Ω, is related to $p(\vec{r})$ by

$$\Omega(\vec{r}) = p(\vec{r})\Omega_{tot} \tag{22}$$

where Ω_{tot} is the total number of possible conformations for a chain with N links. The exact number of Ω_{tot} does not matter for our purposes when we calculate the entropy, S, of the chain, as it is independent of the end-to-end distance.

$$S(\vec{r}) = k_B \ln \Omega(\vec{r}) = S_0 - \frac{3k_B r^2}{2Nb^2} \tag{23}$$

Here, S_0 is a constant where the end-to-end independent contributions are collected and k_B is Boltzmann's constant. Equation 23 shows that extending the chain reduces its entropy. As the end-to-end distance increases, the number of ways the segments can be oriented to achieve the specified separation have to decrease because the fully extended chain is only obtained when the segments are perfectly aligned. Since the segments in the FJC model do not interact with each other, the internal energy of the chain is also independent of the chain extension and can be treated as a constant, U_0. The Helmholtz free energy is then,

$$A = U - TS = U_0 + \frac{3k_B T r^2}{2Nb^2} - TS_0 \tag{24}$$

The expression shows that the minimum free energy is obtained when $r^2 = 0$, which agrees with the calculated mean value, and increases with larger end-to-end distances. Equation 24 also suggests that in order to extend the chain in a certain direction and hold it there, work has to be performed on the system. The force that has to be applied to the ends in order to extend the molecule is given by the derivative of the free energy with respect to the end-to-end distance,

$$\vec{F} = \frac{\partial A}{\partial \vec{r}} = \frac{3k_B T \vec{r}}{Nb^2} = k\vec{r} \tag{25}$$

thus the Gaussian distribution gives a polymer that behaves like a linear spring, which becomes stiffer with increasing temperature, T. However, the entropic elasticity given here is only valid for very weak forces due to a few assumptions made when deriving the Gaussian distribution. These assumptions give negligible errors for large N and $|\vec{r}_N| \ll Nb$, which are the conditions for the distribution, but become significant as the end-to-end distance approaches the contour length [36]. In the force expression

of equation 25, forces where $F > 3k_B T/b$ will result in an end-to-end distance longer than the contour length of the polymer. To be able to model large extensions, the exact partition function for the FJC must be used [37]. The derivation is beyond the scope of this thesis, but once it is done the entropy and the free energy can be calculated in the same way as before. The force derivative of the free energy gives an expression for the extension of a FJC in the direction of the applied force, z, as

$$\frac{z}{L} = \coth\left(\frac{Fb}{k_B T}\right) - \frac{k_B T}{Fb}, \tag{26}$$

where $L = Nb$ is the contour length of the polymer as before. For small forces $F \ll k_B T/b$, the expression gives the same linear force response as with the Gaussian distribution. For large forces $F \gg k_B T/b$, the extension asymptotically approaches the contour length with increasing force as

$$\frac{z}{L} = 1 - \frac{k_B T}{Fb}, \tag{27}$$

which makes more sense for a chain of a fixed length.

3.2.2 The Kratky-Porod wormlike chain

The second polymer model often used to describe DNA is the wormlike chain model (WLC). Semiflexible polymers, such as double-stranded (ds) DNA, are better modeled as thin flexible rods as they are rigid over distances much longer than their monomers. In the wormlike chain model each point, s, on the polymer is described by a position vector $\vec{r}(s)$, and a unit size tangent vector $\vec{u}(s)$ (see Figure 14) where

$$\vec{u}(s) = \frac{d\vec{r}(s)}{ds}. \tag{28}$$

The curvature along the polymer is then described by $d\vec{u}(s)/ds$, which is reduced to a constant for a straight rod. Kratky and Porod [38] demonstrated that the correlation between the tangent vectors at two points along the polymer separated by a distance $|s - s'|$ decays exponentially with increasing distance as
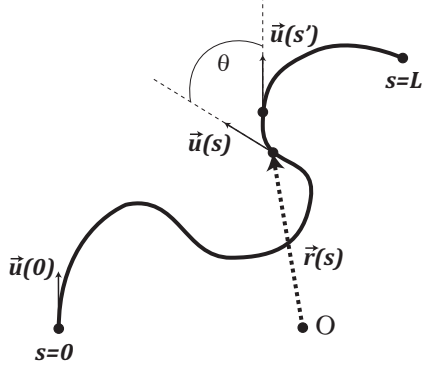
Figure 14 – In the wormlike chain model, the polymer is approximated as an infinitely thin continous wire of length L. Each point, s, on the wire is described by a vector $\vec{r}(s)$ for the position of the point, and a tangent vector $\vec{u}(s)$ that gives the orientation of the wire at the same point. The derivative of the tangent vector describes the curvature along the polymer.

$$\langle \vec{u}(s) \cdot \vec{u}(s') \rangle = \exp\left(-\frac{|s - s'|}{P}\right) \tag{29}$$

The parameter P is the persistence length which defines the characteristic length over which the directionality of the polymer is lost. Thus, P is a measure of the polymer stiffness. A stiff polymer has a long persistence length and maintains its directionality over longer distances than a soft polymer which bends more easily. The persistence length is also related to the bending modulus, B, of the polymer material as [39]

$$P = \frac{B}{k_B T} \tag{30}$$

The energy needed to bend an elastic rod of length L, by an angle θ (Figure 15) is

$$U_{bend} = \frac{B}{2L}\theta^2 \rightarrow \frac{U_{bend}}{k_B T} = \frac{P}{2L}\theta^2 = \frac{P}{2}\int_0^L \left|\frac{d\vec{u}(s)}{ds}\right|^2 ds \tag{31}$$

The persistence length thus relates the bending stiffness of the polymer chain to the thermal energy. Using the definition of P, the mean-square end-to-end distance can be calculated as [39]
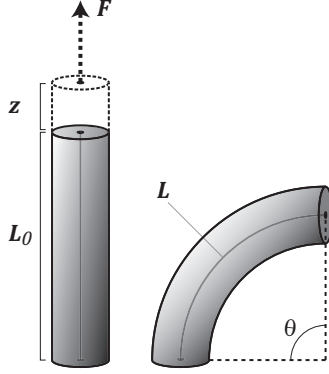
Figure 15 – Stretching and bending of a rod. (Left) Stretching by applying a force F extends the elastic rod by an amount z from its unpertubed length L_0. (Right) Bending a rod of length L, by an angle θ.

$$\langle r^2 \rangle = \int_0^L ds \int_0^L ds' \exp\left(-\frac{|s - s'|}{P}\right) = 2PL - 2P^2\left[1 - \exp\left(-\frac{L}{P}\right)\right]. \qquad (32)$$

The procedure is analogous to the one for the FJC model, but since the WLC model is continuous the sums have been replaced by integrals, and the correlation is substituted with Equation 29. In the limit of $L \gg P$, the second term vanishes and

$$\langle r^2 \rangle \approx 2PL \qquad (33)$$

A comparison with equation 18 shows that the result is the same as in the FJC model with a Kuhn length of $b = 2P$. In the other limit $L \ll P$, where the persistence length is much longer than the length of the polymer, equation 32 is reduced to $\langle r^2 \rangle \approx L^2$, i.e. a polymer much shorter than its persistence length behaves as a stiff rod. When the polymer is of the same length as its persistence length, $L = P$, we get $\langle r^2 \rangle = P^2 2e^{-1}$ or a root-mean-square (rms) end-to-end distance that is about 86% of P [40]. The persistence length of dsDNA varies depending on the solution conditions but is often taken to be about 50 nm [41]. Comparing this value to the average rise per base pair of 0.34 nm shows that dsDNA is a relatively stiff polymer and motivates the description of it as a wormlike chain.

The free energy needed to separate the two ends of a WLC by a small amount $z \ll L$, is the same as in the FJC model (equation 24) with $Nb^2 = Lb = 2PL$,

$$\Delta A = 3k_B T z^2/(4PL). \qquad (34)$$

Thus at forces below the characteristic force of $F_c = k_B T / P$ where the extension in the direction of the applied tension is small compared to the contour length, the force response is again linear.

$$F = \frac{\partial A}{\partial z} = \frac{3k_B T z}{2PL} \tag{35}$$

The high force $(F \gg F_c)$ response of the wormlike chain model can be derived from the Boltzmann distribution of the bending energy (Equation 31) with the added work term $-Fz$ [42].

$$F = \frac{k_B T}{4P(1 - z/L)^2} \quad \rightarrow \quad \frac{z}{L} = 1 - \frac{1}{\sqrt{4PF/k_B T}} \tag{36}$$

The result establishes that for large forces the extension in the WLC model approaches the contour length as $1/\sqrt{F}$, which can be compared to the high force behavior of a freely jointed chain (equation 27), where $L - z \propto 1/F$. The exact force response over all extensions of a wormlike chain can only be solved numerically. However, a useful approximate interpolation formula has been derived to describe the force versus extension relation [42].

$$F = \frac{k_B T}{P} \left[\frac{z}{L} + \frac{1}{4(1 - z/L)^2} - \frac{1}{4} \right] \tag{37}$$

Equation 37 is a combination of the high and low force behaviors, and is asymptotically exact in both limits. In Figure 16 the force-extension relation of the two models is plotted in a reduced form to show the differences between them. The figure illustrates how both models behave as linear springs at low forces while at high forces and equivalent parameters $(b = 2P)$ the wormlike chain is significantly stiffer.
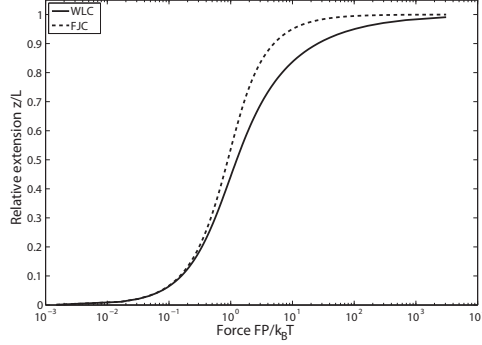
Figure 16 – The relative extension as a function of force for the wormlike chain (WLC) and the freely jointed chain (FJC) models. The comparison is made with $b = 2P$.

3.2.3 Applying the models to force spectroscopy of DNA

How well do the presented models work when applied in high force DNA stretching experiments? The answer to the question is that they actually describe the DNA quite poorly in the forms stated above. However, they do provide a good starting point. The models can describe the force-extension relation of DNA reasonably well for small extensions, but become inaccurate at extensions approaching the contour length. The reason for the failure of the pure WLC and FJC models is mainly caused by the assumption of a fixed contour length. If we again consider an elastic rod of length L_0 with a circular cross section of radius r_r and apply a force at the ends in the direction of the length axis to stretch it by an amount z. For small extensions the deformation is linear and follow Hooke's law such that

$$F = \frac{Y\pi r_r^2}{L_0} z = K\frac{z}{L_0},\tag{38}$$

where Y is Young's modulus that characterizes the resistance toward stretching or compression of the rod material. The elastic constant $K = Y \times$ *cross section area*, is a convenient substitution and has the dimensions of force. The energy needed to stretch the rod is then

$$U_{stretch} = \int_0^z F dz = \frac{K}{L_0}\int_0^z z dz = \frac{Kz^2}{2L_0}\tag{39}$$

Relaxing the constraint of a fixed contour length in the WLC by the addition of a linear stretching elasticity gives an extensible wormlike chain model (ExWLC) [43].
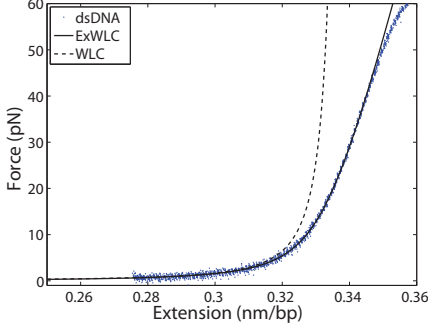
Figure 17 - The figure shows the failure of the inextensible WLC model to describe high force stretching of dsDNA. The blue curve is force-extension data for a 12 kbp dsDNA molecule stretched in 1 M NaCl. The dotted line is the wormlike chain model (WLC) with $L_0 = 0.34$ nm/bp, $P = 46$ nm and $T = 296$ K. The solid line shows the extensible wormlike chain model (ExWLC) with the same parameters and $K = 1050$ pN. The inextensible WLC model describes the force vs. extension relation of dsDNA reasonably well up to a few pN.

$$\frac{z}{L_0} = 1 - \frac{1}{2}\left(\frac{k_B T}{FP}\right)^{1/2} + \frac{F}{K} \tag{40}$$

Figure 17 plots the force vs. extension relations for both the inextensible and the extensible wormlike chain models together with stretching data from a 12 kbp double-stranded DNA molecule. The figure shows how the WLC model starts to deviate from the measured data at extensions approaching the zero-force contour length. The ExWLC model on the other hand is able to describe the elasticity of dsDNA up to about 50 pN before failing.

The FJC model is not suitable for describing double-stranded DNA [44], but can be used for single-stranded (ss) DNA which is more flexible. As for the WLC model, the extensibility of the backbone has to be accounted for in order to capture the behavior at higher forces [45].

$$\frac{z}{L_0} = \left[\coth\left(\frac{Fb}{k_B T}\right) - \frac{k_B T}{Fb}\right]\left(1 + \frac{F}{K}\right) \tag{41}$$

Measurements from ssDNA stretching experiments at pH 8, and a Na⁺ concentration of 150 mM have resulted in values fitted to Equation 41 of $L_0 = 0.56$ nm/bp, $b = 1.5$ nm, and $K = 800$ pN [45].

3.2.4 Counterion-influence on the mechanics of DNA

The large persistence length of dsDNA can be attributed to both the double-helical conformation, which restricts many bond angles within the duplex, and the polyanionic nature of the backbones. The negative charges of the phosphodiester

groups repel each other both within a single strand and between strands. The charged phosphodiester groups attract cationic counterions present in the solvent which screens the electrostatic repulsion and thereby reduces the effective charge of the strands. The screening from counterions effectively reduces the persistence length of the DNA making it more flexible as the electrostatic repulsion within the backbone is reduced. Hence, the ionic strength of the solvent is an important parameter when studying DNA mechanics [41].

Several theories exist that are useful for explaining how ions in the buffer interact with polyelectrolytes such as DNA. Counterion condensation theory provides a relatively simplistic model for how the net charge of a polymer is affected by ions present in the surrounding medium [46, 47]. The model treats the charged polymer as a locally straight line with a continuous charge density. The distance over which the charge of the polymer is screened by counterions in the solution is called the Debye length, usually denoted in the inverse form as κ^{-1}. The Debye length depends on the ionic strength of the solvent, I, and is calculated as $\kappa^{-1} = 1/\sqrt{8\pi N_A b_j I}$, where N_A is Avogadro's number and b_j the Bjerrum length. The Bjerrum length is the distance between two unit charges at which the Coulomb energy equals the thermal energy, and is given by $b_j = q^2/(4\pi\varepsilon_0\varepsilon_r k_B T)$ Here q is the elementary charge, ε_r the relative dielectric constant of the medium, ε_0 the vacuum permittivity, and gives a value of $b_j \approx 0.7$ nm in water at room temperature. The charge density in counterion condensation theory is defined by the linear spacing of the charges, l_c, in the modeled polymer. For B-form DNA, $l_c = 0.17$ nm as there are two negative charges per base pair. The theory defines a charge density parameter $\xi = b_j/l_c$ and states that if $\xi > 1$ ($\xi_{dsDNA} = 4.2$), counterions will condense onto the polymer until the effective value of ξ is reduced to unity. The condensed counterions stay closely associated with the polymer and reduce the net charge by a factor of $1 - 1/N\xi$, where N is the valence number of the condensed ions [41].

The electrostatic effect on the persistence length is commonly described using the Odijk-Skolnick-Fixman (OSF) theory [48, 49]. The theory applies the Debye-Hückel approximation to evaluate the electrostatic contribution to the bending energy of a wormlike chain. The result is a separation of the persistence length into two parts as

$$P = P_0 + P_{el}, \tag{42}$$

where the total persistence length is the sum of an intrinsic part, P_0, for the uncharged chain, and a contribution, P_{el}, accounting for the electrostatic interactions.

The theory predicts that for a densely charged polyelectrolyte such as dsDNA, P_{el} should vary with the molar ionic strength of the solvent as [50]

$$P_{el} = \frac{1}{4\kappa^2 b_j} = 0.0324/I[M] \text{ nm.} \tag{43}$$

This provides a rough estimate for how the persistence length is affected by the counterion concentration. Measurements by Wenner et al [51] show that the persistence length of dsDNA is increased from 46±2 nm, at a Na+ concentration of 1 M, to 59±2 nm when the concentration is lowered to 2.6 mM. For a solid circular rod of an isotropic material, the bending modulus and Young's modulus are related as $B = Y\pi r_r^4/4$ or equivalently the persistence length to the stretch coefficient, K, as $P = Kr_r^2/(4k_B T)$ [52]. This suggests that it is possible to estimate K from the persistence length and that the value of K should increase with decreasing ionic strength, as for P. Calculations based on these assumptions slightly underestimate the value of K for reasonable values of the rod radius, and measurements of the ionic strength dependence of K showed that it actually was fairly constant or decreased somewhat with lower ionic strengths [45, 50, 53]. This inconsistency was resolved in a renormalization model by Podgornik et al that accounted for the electrostatic interactions of the backbones [54]. The predicted weak ionic strength dependence of K for double-stranded DNA was confirmed together with the measurements of the persistence length in the previously cited paper by Wenner et al [51]. Several groups have measured the elasticity of dsDNA, and found that the typical value of K is about 1000-1300 pN [45, 50, 51, 53, 55].

Even with electrostatic effects accounted for, the elasticity of dsDNA is significantly more complex than that of a simple rod. Experiments measuring the rate of circle formation in oligonucleotides of about 60-200 bp have shown that dsDNA can be much more flexible than predicted for a simple wormlike chain [40, 56-59]. Modified versions of the WLC model that accounts for the abnormal bending elasticity as either temporary melting bubbles [60] or kinks [61, 62] in the DNA helix have been suggested. However, many of the results remain controversial [63]. Even if dsDNA locally may be more flexible when free in solution, an applied stretching force in the sub-pN range will likely render these bending configurations inaccessible [58], and thus have a limited impact on high force stretching experiments.

3.3 Stretching and overstretching DNA

3.3.1 Early accounts of DNA extensibility

The idea that double-stranded DNA can be extended beyond the contour length of the relaxed state is certainly not new. In 1951, even before the double-helical structure of DNA was known, Wilkins, Gosling, and Seeds suggested that nucleic acid fibers were extensible [64]. In their experiments they noted that the optical properties of the fibers changed as they were stretched, and concluded that the fibers underwent a transition into a longer form which could be stretched to roughly twice the original length before breaking. However, the story of the overstretching transition really begins with the emergence of techniques where individual DNA molecules could be studied.

Development of atomic force microscopy (AFM) and advances in fluorescence microscopy in the 1980's and early 90's resulted in visualizations of single DNA molecules and that behaviors different from those of the bulk of the population could be observed [10, 65-71]. In 1993, while developing a technique for optical mapping of genomes, Parra and Windle deposited droplets of fluorescently stained DNA on glass slides [72]. In order to align the molecules on the surface, the slide was tilted and the droplets were allowed to run down the length of the slide. While examining the deposited DNA they noticed that some of the molecules appeared to have been extended by up to twice the expected length. Slightly larger extensions of up to 2.14 times the B-form contour length were observed by Bensimon et al. in experiments where they deposited stained DNA on a surface and allowed the receding meniscus of the evaporating droplet to align the DNA [73]. A similar approach was used in 1994 by Thundat et al. to fixate DNA on mica surfaces for AFM imaging [74]. They discovered that the deposited DNA strands frequently were trapped in elongated forms up to 1.8 times the natural contour length and that the diameter of these extended molecules was reduced by ~50%. The suggested explanation was that the DNA helix was uncoiled as the molecule was stretched. A simple model for explaining dsDNA extensions of ~two times the B-form length is to think about the DNA helix as a wire wrapped around the surface of a cylinder that is unwrapped in response to stretching. Given that dsDNA in the B-form has a diameter of about 2 nm and a helical repeat of 3.4 nm (10 bp), the fully uncoiled helix would be $((2\pi)^2 + 3.4^2)^{1/2}$=7.1 nm or 2.1 times the B-form contour length.

3.3.2 DNA force-spectroscopy using single-molecule techniques

At around the same time as the above-mentioned deposition experiments, various methods for performing controlled single-molecule force manipulation were being developed and applied to the field of DNA elasticity [10, 44, 75, 76]. By attaching one end of a DNA molecule to the surface of a glass slide and the other to a micrometer sized magnetic bead, Smith et al [44] were able to directly measure the elasticity of a single DNA molecule as a function of force. The force on the tethered bead was generated by a set of movable magnets together with a variable flow in the chamber. In combination this set up allowed applied forces between ~0.01 and 40 pN to be explored. The results showed that in the lower end of this force regime, the DNA behaved much as expected for a long semi-flexible polymer with a persistence length of about 50 nm (150 bp) [77]. However, for high forces the end-to-end distance deviated from the expected approach toward the contour length as $1/\sqrt{F}$. This was remedied by adding the intrinsic elasticity parameter to the wormlike chain model that reflects the increase in contour length as the polymer is deformed under tension [42, 43]. When forces of about 60-70 pN were applied to double-stranded DNA in these types of force-measuring single-molecule experiments it was discovered that the molecules underwent a cooperative transition during which the contour length of the DNA was increased by up to about 1.7 times that of the unstressed B-form configuration [45, 78, 79]. This force-induced structural transition of the double-stranded DNA molecule is the so called overstretching transition. Figure 18 show the overstretching transition for a 12 kbp DNA molecule when stretched in 1 M NaCl.

In February 1996, two papers were published in the same issue of Science showing how DNA can be overstretched using force-measuring single-molecule techniques. Cluzel et al [79], used an approach where they attached a DNA molecule between the tip of an optical fiber and a polystyrene bead immobilized on a piezo-controlled micropipette. The DNA molecule was stretched by moving the micropipette and the resulting tension was inferred from the bending stiffness of the calibrated optical fiber, similar to how force is measured in AFM. This setup allowed establishment of the relationship between force and extension for forces of up to 160 pN. In addition to the *in vitro* stretching experiments, the group also performed molecular mechanics stretching simulations suggesting that the DNA conformation formed during the overstretching transition could still be base-paired. This new stretched DNA structure was named 'S-form'.
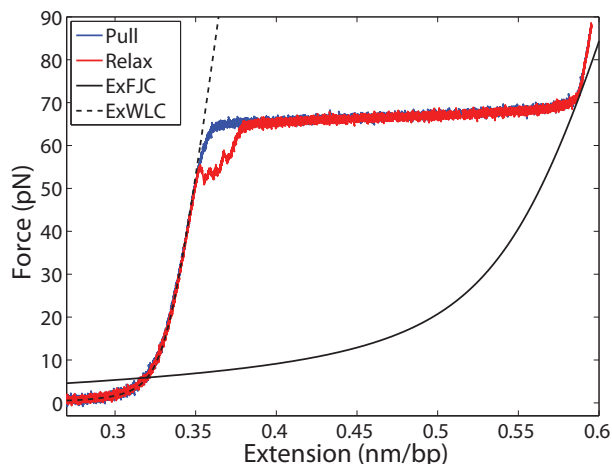
Figure 18 – The overstretching transition in torsionally unconstrained dsDNA that is stretched by its ends. The figure shows force as a function of extension per base pair for a 12 kbp dsDNA molecule (fragment from bacteriophage λ, 47% GC) stretched in 1 M NaCl (pH 7.4). The blue curve is the pulling of the molecule as the force is increased, while the red curve shows the relaxation of the molecule as the applied force is reduced. The dotted line is the extensible wormlike chain model (ExWLC) and the solid line the extensible freely jointed chain model (ExFJC) for single stranded DNA with the same number of bases.

In the second Science paper, Smith et al [45] overstretched DNA using optical tweezers and reached a similar conclusion. When they stretched DNA in 150 mM NaCl a force – extension curve qualitatively identical to what Cluzel and co-workers observed was obtained. However, during relaxation of the stretched DNA molecules they often observed that the transition was not fully reversible, i.e. the curve measured during relaxation differed from the one during stretching. This hysteresis, where the force during relaxation is lower than during the stretching phase at a given extension of the molecule, indicated that the DNA was partially melted during the transition. Hysteresis can be observed, see Figure 18, as the difference between pulling curve (blue) and the relaxation curve (red). The difference between the curves disappeared when the DNA strands were cross-linked using psoralen, which suggested that the hysteresis was indeed due to slow rehybridization of frayed strands. The hysteresis was also mostly removed by increasing the Na+ concentration to 1 M, without any major change to the transition force or the cooperativity of the process. These results, and the fact that DNA did not come apart at the end of the transition even though it was being pulled by the 3'-ends of the opposite strands, led to the conclusion that most of the base-pairing between the two strands remains intact during the overstretching transition. When comparing the force – extension

profiles of dsDNA and ssDNA one finds that at low forces (a few pN) dsDNA is more extended than ssDNA due to a longer persistence length, while at high forces this relation is the opposite. Another important observation is that at the end of the overstretching transition the two curves are very close to each other (see Figure 18).

The results from these single-DNA overstretching experiments were quickly followed by theoretical models for the transition [80, 81], and computational studies that supported the existence of S-form DNA [82-84]. While the studies showed differences, they all suggested that it was possible to extend dsDNA to lengths observed in experiments, while retaining most of the base pair hydrogen bonds. The study by Lebrun and Lavery [82] also suggested that the way the tension is applied is of importance for the structure of the S-form. They found that if the modeled DNA molecule was pulled by the 3'-ends of opposite strands (3'-to-3') it would extend from its B-form state by unstacking and unwinding into a ladder-like form, which also was the result of the other computational studies. If instead the tension was applied to the 5'-ends of the molecule (5'-to-5'), or to both ends of one strand (5'-to-3'), the DNA molecule was predicted to respond by reducing the radius of the helix to accommodate the extension. However, while the simulations qualitatively agreed with experimental results for the overstretching transition and could reproduce a cooperative reversible transition, the calculated stretching energies were generally significantly higher than those estimated from experiments.
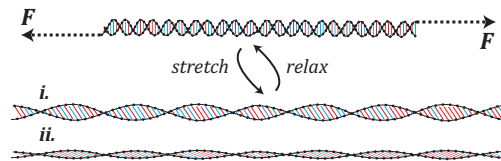
Figure 19 – The two proposed types of S-form. (*i.*) Unwound ladder when pulling 3'-to-3' . (*ii.*) Reduced radius fiber when pulling 5'-to-5' or 5'-to-3'.

By using AFM to stretch dsDNA adsorbed onto a gold surface, Gaub and coworkers were able to study the force – extension relation at even higher forces [85, 86]. The results showed that the overstretching transition for mixed sequence DNA at ~65 pN is followed by a second transition at ~150 pN where the DNA is completely melted. In contrast to the first overstretching transition, the second transition was a nonequilibrium process as it was sensitive to the rate at which the force was applied during the experiment. This suggested, by way of contrast, that the overstretching at ~65 pN was primarily a transition to S-form DNA and not force-induced strand-separation. In their experiments they also examined the sequence dependence of the transitions by stretching poly(dG-dC) and poly(dA-dT) DNA. The

results revealed that poly(dG-dC) overstretched at ~65 pN followed by a non-cooperative melting transition starting at ~250 pN. Poly(dA-dT) on the other hand displayed a plateau in the force – extension curve at about 35 pN that was determined to be force-induced melting of the strands, where one strand is progressively peeled off the other. The experimental protocol allowed forces of up to 800 pN to be applied to the DNA and showed that the covalent bonds of the sugar-phosphate backbone are stable at forces of this magnitude. The stability of the DNA backbone was also estimated in the previously mentioned receding meniscus experiments by Bensimon et al [73]. They calculated that the force needed to break the covalent bonds of the DNA backbone was about 480 pN, this was however based on an early Young's modulus value for DNA of 1.1×10^8 Pa [87]. Estimates of Young's modulus from single-molecule force-spectroscopy measurements put the breaking force in the nanonewton range. Other AFM measurements on short dsDNA indicated that the breaking force is over 1.7 nN [88], in line with the measured stability of other types of covalent bonds [89]. To define a single force needed to break the backbone is difficult since it depends on several factors such as the rate of stretching, the solvent, and how long the molecule is (how many bonds that can potentially be broken).

3.3.3 Twisting and pulling

The overstretching transition at around 60 - 70 pN is what occurs when a torsionally unconstrained DNA molecule is stretched, i.e. when it can rotate freely around its own length axis. This is the case in any stretching experiment where the DNA contains a nick in the backbone or where the attachment points allow free rotation. However, if rotation is somehow prohibited by the attachment strategy, also stretching at which the torsion is constrained or controlled can be studied [90-93]. As higher forces became available in single molecule force experiments, it was shown that torsionally constrained DNA could be overstretched by applying ~110 pN, which was in agreement with theoretical predictions [86, 94-96]. If the DNA is underwound (left-handed or negative torque) before it is stretched, it will transition into a state with a negative average twist called "Z"-DNA [96, 97] or L-DNA [93, 98] with a length similar to B-form DNA. In this state bases are known to be exposed to the solvent[99], which implies at least partial melting. When L-DNA is stretched, the extension curve exhibits two transitions, one at ~50 pN, where the portion of the DNA that is L-form is overstretched, and then another at ~110 pN where the remaining B-form is overstretched [98]. The ratio between how much of the overstretching that occurs at the two transitions depends on the amount of unwinding, with more of the transition occurring at ~50 pN with increasing amount

of unwinding. Pure L-DNA does not exhibit any cooperative stretching transitions [96]. If the DNA is overwound by applying a positive torque (right-handed) it was found that it transitions into a longer form with increased helicity. The data suggested that this overwound state corresponded to an inversion of the helix where the bases are pointing out into the solvent from wound backbones [92, 96]. The structure was named Pauling DNA (P-DNA) due to the similarity to the structure for DNA that was proposed by Linus Pauling in 1953 [100]. At low tensions (~< 25 pN) the overwound DNA forms plectonemic supercoils (scP). Figure 20 shows a Force-Torque 'phase-diagram' that was proposed by Sarkar et al [97] to describe the transitions between these states. In an experiment by Gore et al the twist of the DNA was monitored during stretching using a small rotor bead attached along the molecule [101]. The results revealed that while high forces induced unwinding of the DNA, stretching forces up to about 30 pN actually overwinds it. This complex twist-stretch coupling of dsDNA, together with the other results, clearly demonstrates that the mechanical properties of the molecule are very different from those of an isotropic rod.
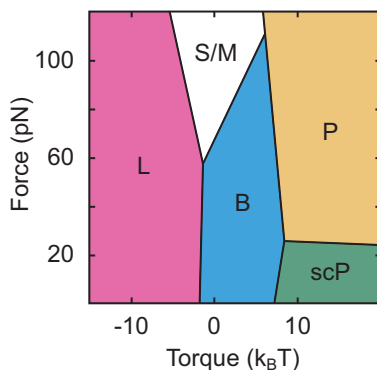
Figure 20 - Force – Torque 'phase diagram', adapted from [97]. The diagram illustrates how B-form DNA changes structure with applied tension and torque. The lines separating the regions are an indication of conditions where phases coexist. S/M: overstretched, L: underwound "left-handed", P: overwound Pauling, sc: supercoiled

3.3.4 The overstretching transition as force-induced melting

In 2001, a new model for the overstretching transition was proposed by Rouzina and Bloomfield [102, 103]. The model was based on a thermodynamic analysis of the transition and argued that overstretching could be completely explained simply in terms of force-induced melting of the DNA, without introducing any novel base-

paired stretched state as the S-form. As the DNA molecule is overstretched it is progressively converted from double-stranded into single-stranded form, breaking both base stacking and hydrogen bonding between the bases by the work performed on the DNA molecule during stretching.

At free ends, such as sites where one strand is nicked or at the ends of the polymer, the transition will lead to a single-stranded state where one strand is peeled off from the other leaving all the tension on one strand while the other is relaxed. This peeling process will continue as the molecule is stretched until it reaches a region of higher stability. Between these more stable regions, the DNA is also progressively melted with further extension of the molecule in the transition. In the internally melted regions the two single-strands formed still remain close to each other and the tension is shared between them. Figure 21 illustrates the two types of force-induced melting.
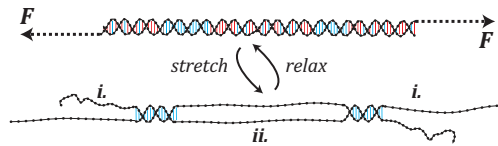

Figure 21 – The two types of force-induced melting occuring during overstretching. Extension of the DNA is accomodated by progressively disrupting the B-form helix and forming ssDNA. The process can be divided into two types where the main difference is how the tension is divided between the two released strands. (*i.*) Peeling of one strand off the other at free ends. (*ii.*) Internal melting of regions within the sequence.

The thermodynamic aspect of the model can be understood by comparison of the force – extension curves for double-stranded B-form DNA and single-stranded DNA (see Figure 18). At high forces, the average end-to-end distance of ssDNA is longer than that of dsDNA at the same force, and thus stretching will reduce the free energy difference between the two states. This also implies that at forces below the crossing point of the two curves, stretching stabilizes the dsDNA. The fact that DNA does not immediately dissociate at the end of the overstretching plateau when the tension is applied to opposite strands - one of the main arguments for introducing S-form DNA - was explained by the one-dimensional nature of the melting process. This means that at any point in the transition there will be a number of boundaries between double-stranded and single-stranded DNA that at equilibrium defines the average size of these regions. As the force is increased the average size of the single-stranded domains will grow at the expense of the double-stranded regions, and complete dissociation of the two strands will not occur until the average size of

the melted regions reaches the full length of the polymer [102]. According to this the authors estimated that a 10 kb long DNA molecule should withstand forces up to ~100 pN, and a 1 kb molecule forces up to ~80 pN. The melting of the remaining double-stranded regions would be a non-equilibrium process and thus depend on the loading rate (the rate of change of the applied force), as indeed observed in experiments [85, 86, 104]. The force-induced melting model was further strengthened by experiments where the overstretching force, taken as the force needed to stretch the DNA half-way through the overstretching transition, was measured as a function of pH [105], ionic strength [51], and temperature [106]. These studies all showed that solvent conditions known to destabilize dsDNA in bulk experiments also reduced the force needed to overstretch the DNA, in agreement with the proposed model. The measurements of the salt dependence also suggested that the two strands remain close to each other during the transition, which in the context of force-induced melting implies that melting primarily occurs internally rather than from free ends.

3.3.5   S-DNA persists

Using a similar thermodynamic approach to analyze the available data, Cocco et al arrived at a different conclusion regarding the structure of overstretched DNA [107]. In their analysis they estimated the free energy of overstretched DNA and compared it with the two cases of force-melted DNA. The authors conclude that at neutral pH, room temperature, and sodium chloride concentrations of 150 mM (and above), the overstretching transition observed for mixed sequence DNA at ~65 pN is predominantly conversion of B-form DNA into S-form. While peeling from a free end is favorable at the transition force for moderately AT-rich sequences, GC-rich regions were calculated to need up to 150 pN to separate. This would prevent peeling at any larger scale to occur as it would quickly stall at GC-rich regions. Internal melting was calculated to only begin to be favorable at the transition force, and thus be preceded by both peeling and S-form formation. The authors also argued that the measured elasticity of overstretched DNA at forces above the transition could not be explained by force-induced melting. Put simply, overstretched DNA exhibits a significantly stiffer force response than that of either one strand of DNA, two parallel non-interacting strands, or B-form at the same elongation. If the resulting overstretched DNA was a mixture of these forms, then the effective elasticity should be a linear combination of the respective elasticities. However, the results showed that force-induced melting is favored over S-DNA formation under low salt conditions. These conclusions were qualitatively supported in another modeling study by Storm and Nelson who also reached the conclusion that the overstretched state

has a bending stiffness that is between that of B-form and two single strands, but with a substantially larger stretch modulus [108].

3.3.6 Ligands, modifications and kinetics

In an effort to directly probe the structure of the overstretched DNA, Shokri et al performed stretching experiments in the presence of the dialdehyde glyoxal [109]. Glyoxal can be used to detect melting of dsDNA as it strongly binds to guanine bases in the formed ssDNA and prevents rehybridization (see section 3.4.3). The results showed that the overstretched DNA was significantly modified by the glyoxal, suggesting that the transition involves extensive melting of the duplex. The results also established that exposure at forces below the transition plateau did not modify the DNA, which indicates that the melting indeed is a result of the applied force and not induced by the glyoxal. Glyoxal was also used to probe the overstretched state in a study where the effect of different pulling geometries was investigated. In the performed experiments the DNA was overstretched by either applying the force 3'-to-3', 5'-to-5', or 5'-to-3' [110]. The results led to the conclusion that the force needed to completely melt the DNA differed depending on how the force was applied. A similar result was obtained in a study when different pulling modes were applied to DNA only 30 bp long [111], suggesting that the structure of the overstretched DNA is different between the cases as predicted by Lebrun and Lavery [82].

By combining optical tweezers and fluorescence microscopy, van Mameren et al were able to visualize the structural changes that occur during the overstretching transition [112]. Using fluorescent single-strand binding proteins and an intercalating dye they found that the overstretching at about 65 pN of torsionally unconstrained DNA was mainly a peeling transition, while the transition at ~110 pN of constrained DNA was a result of internal melting. Another study where the fluorescence polarization of the intercalating dye was measured during unconstrained overstretching confirmed the interpretation of the transition as force-induced melting, as the polarization measurement did not indicate any signs of the base tilting expected for S-form DNA [113].

In contrast to this evidence, studies where the kinetics of the overstretching where followed, suggested that the transition was a combination of one fast B-to-S-form transition and one slow transition corresponding to the gradual melting by end-initiated peeling [114-116]. A report by Paik and Perkins also showed that a topologically closed but unconstrained DNA-construct containing no free ends could

be overstretched without any significant change to the transition [117]. Thus peeling is not the only process through which overstretching can occur. AFM imaging of DNA stretched on a coated glass surface, showed regions in the polymers with a reduced diameter and a regular helical pitch, indicating an S-form like structure [118]. The many seemingly conflicting results presented in this section provide the background against which the work in this thesis was performed.

3.4   Methods used for modifying and probing DNA

3.4.1   Cu(I)-catalyzed click chemistry to inhibit melting

The concept of "click chemistry" was coined by Sharpless and coworkers in 2001 [119]. To qualify as click chemistry, a reaction has to follow certain criteria; the reaction has to give very high yields of a stereospecific product with only "inoffensive" byproducts, and it should work in a benign solvent like water. Furthermore, the product should be stable under physiological conditions and be simple to isolate. A reaction that fulfills most of the stated criteria is the copper(I)-catalyzed 1,3-cycloaddition of an azide and a terminal alkyne. The reaction (Figure 22) selectively forms a 1,4-disubstituted 1,2,3-triazole, and can be performed in water at room temperature with nearly quantitative yields.
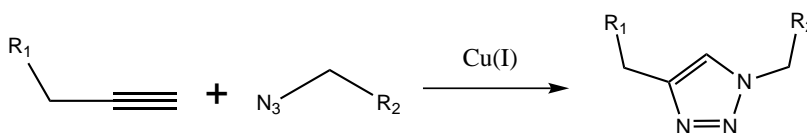
Figure 22 – The Cu(I)-catalyzed 1,3-dipolar cycloaddition (CuAAC)

The reaction is also known as CuAAC, and was discovered independently by Meldal [120] and Sharpless [121] in 2002. The exact details of the reaction are not fully understood but a plausible mechanism has been proposed [122]. The active form of copper in the reaction is Cu(I), which usually is generated from Cu(II)-salts *in situ* by a reducing agent. When the reaction is performed in water, sodium ascorbate is often used to reduce the copper, and is typically added in excess to ensure that it remains reduced [121]. The reaction rate can be increased by adding a ligand that coordinates to the reduced copper and protects it against oxidation [123]. By introducing nucleotides modified with azides or alkynes during DNA synthesis, the reaction can be used to form covalent links that concatenate [124-126] or cross-link DNA strands [127, 128]. In the works of this thesis, the reaction has been used to introduce site
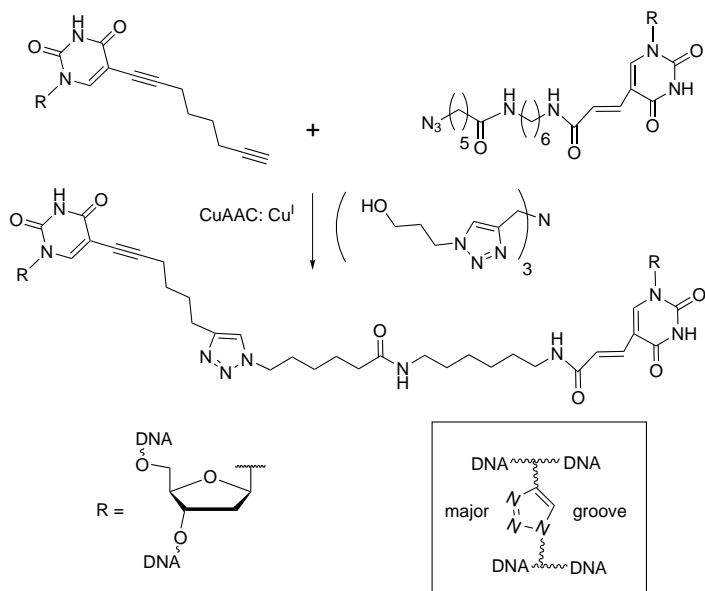
Figure 23 – Bases modified with an alkyne and an azide are covalently linked together to form an inter-strand crosslink.

specific inter-strand crosslinks at one or both ends of oligonucleotide DNA sequences. Such cross-links are known to significantly increase the melting temperature of the modified DNA duplex [128], and have been used as a way of inhibiting strand separation. Figure 23 illustrates the CuAAC reaction where two bases on opposite strands are covalently linked together.

3.4.2   Gel electrophoresis of DNA

The charged nature of DNA means that it can be influenced by an applied electric field, as was discussed in section 3.2.4 (influence of counterions). In this work gel electrophoresis has been used as an analytical tool to evaluate the melting temperature of DNA sequences modified with inter-strand crosslinks. It has also been used as a preparative tool to purify the cross-linked constructs when needed.

In electrophoresis an electric field is used to translate charged particles or molecules through a viscous medium. The most common application of the technique is to separate biological macromolecules such as proteins or DNA, for either analytical or preparative purposes. When the field is applied, the particles will experience a force that accelerates them toward the corresponding electrode. Negatively charged particles and molecules will migrate in the direction of the anode,

while positively charged species will move in the opposite direction to the cathode. The force $F_{el} = QE$, is proportional to the charge of the particle, Q, and the strength of the field, E. In solution small particles quickly reach a steady state velocity as the electric force is balanced by the increasing frictional force, $F_f = f_t v$. The retarding force depends on the translational friction, f_t, between the particle and the surrounding medium, and increases with the velocity v. To make it easier to compare experiments, the velocity is typically divided by electric field strength to give the electrophoretic mobility, μ [41]:

$$\mu = \frac{v}{E} = \frac{Q}{f_t}.$$

(44)

For a given medium, the frictional coefficient f_t will be determined by the size and shape of the molecule. This, together with the charge of the molecule, means that molecules that differ in these respects will migrate at different velocities and can thus be separated by an applied electric field. However, for uniformly charged polymers such as DNA, the charge scales with the size and, thus, cancels the effect of the increased friction. Therefore, electrophoretic separation of different lengths of DNA in free solution is only possible for DNA lengths up to about 400 bp [129]. To be able to separate larger DNA molecules and to enhance the effect, a gel matrix is typically used to increase the frictional discrimination. The differently sized pores formed in the gel hinder the migration of the molecules depending on their size and shape, and separation is again possible. The most commonly used gel matrices are those of agarose and cross-linked polyacrylamide [130]. By adjusting the concentration of agarose or polyacrylamide polymers, the distribution of formed pore sizes can be varied to fit the size range of the analytes that are to be separated.

3.4.3 Detecting strand separation using glyoxal

Glyoxal or ethanedial has a history of being used as a tool for fixating melted regions of DNA [131-133]. The molecule reacts with adenine, cytosine, and guanine bases in DNA that are exposed to the solvent. However, only the reaction with guanine forms a stable product. The glyoxal forms a covalent adduct with the 1,2-amines of the guanine base and thus prevents the base from forming base pair hydrogen bonds with a complementary cytosine [134-136].
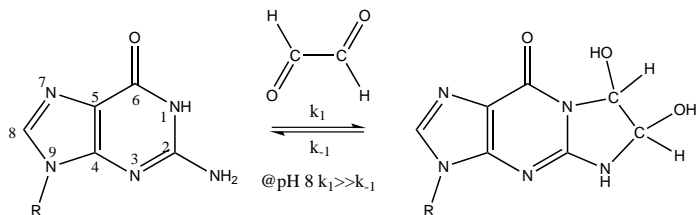
Figure 24 – Glyoxal adduct formation on a guanine base of a nucleotide.

The inability of the glyoxal modified guanine bases to pair with complementary bases has been utilized to map low-melting regions of genomic DNA. By adding glyoxal to the solvent and heating a DNA sample to a few degrees below the average melting temperature, less stable AT-rich regions can selectively be modified as they melt at a lower temperature. As the adduct formation is almost completely irreversible, rehybridization of the modified regions is inhibited. More importantly, modification of double-stranded DNA only occurs to any larger extent when the base-pairing is broken, and can thus be used as a probe to detect such events. Glyoxal has also been used successfully in single molecule force-spectroscopy to detect strand separation [92, 109, 110].

4   Experiments, results, and discussion

The work presented in this thesis is focused on understanding the structural changes that occur during the overstretching transition of double-stranded DNA.

When the project was initiated, the evidence (Section 3.4) suggested that changes in the experimental conditions that reduce the stability of dsDNA also led to force-induced melting during the overstretching transition. Therefore, if the overstretched S-form did exist, it would likely be most stable for GC-rich sequences at high ionic strengths. On the other hand, results supporting an S-form interpretation of the transition questioned the role of internal melting as an important mechanism for overstretching. With the humble aim to finally resolving all these differences, the problem is approached by studying short sequences of double-stranded DNA whose base content can be designed at will. There are several arguments in favour of this approach. By using short DNA, the strands can be synthesized using solid phase techniques which mean that just about any sequence can be studied. During synthesis, modified nucleotides can also be included to alter the structural properties of the DNA. This approach is used to seal the ends of some of the double-stranded sequences by locally forming covalent links between the two strands using the CuAAC reaction.

One of the strongest arguments for studying short DNA is that long genomic DNA typically has inhomogeneous sequences with regions of different stability. As overstretching depends on the stability of the sequence, the transition can then include several different processes at the same time for different parts of the molecule. Resolving the contributions and interactions between regions can quickly become a complex problem as the number of them increases. However, using a short molecule presents other challenges; as the overall length of the molecule is shorter, so is the resulting extension to be measured during the transition. The lower extension signal of a shorter molecule is also coupled to a lower signal-to-noise ratio as the size of the system is reduced.

The strategy of the project can be described as a bottom-up approach, where first the behavior of "monomer"-sequences of about 60 base pairs are studied and then concatenated into "dimers" of about 120 bp. Knowing how the two parts of the dimer behave by themselves enables a more detailed understanding of the transition in the molecule. This chapter provides a summary of performed experiments, the main results, and a discussion of them.
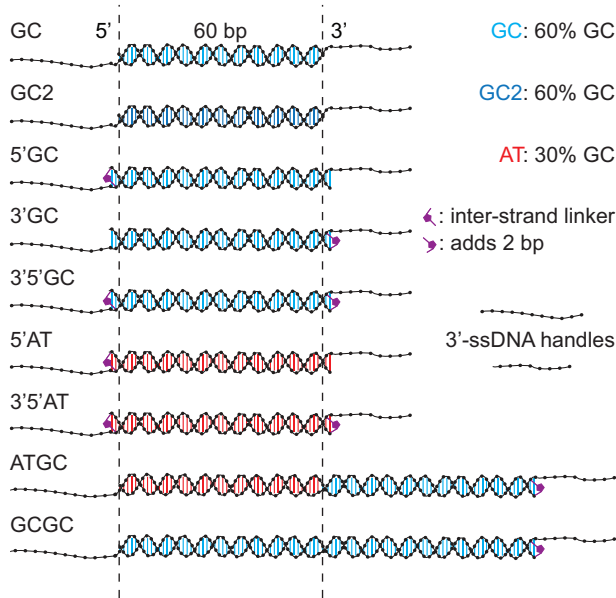
Figure 25 – The studied DNA constructs. Three different 60 bp core sequences were used: GC and GC2, that both have a GC-content of 60% but different sequences, and AT that has a GC-content of 30%. Before hybridizing the double-stranded region, the 3'-ends of the two strands of each construct were extended using terminal transferase to incorporate biotin and digoxigenin labels for bead attachment. Versions of the GC- and AT- sequences were also modified to include inter-strand crosslinkers to inhibit peeling. "Dimers" of the GC and AT sequences were also studied (ATGC & GCGC).

4.1 The studied DNA constructs

Figure 25 gives an overview of the different DNA constructs that were studied. Three 60 bp double-stranded "core" sequences were used: oligonucleotides named GC and AT, that differ in their respective GC-contents (60% and 30% respectively), and GC2 that has the same GC-content as GC but a different nearest-neighbor base composition. Variations of the GC- and AT-sequences were also studied. These included site specific inter-strand crosslinks at one or both ends of the double-stranded regions. The linkers served two purposes: they inhibited peeling of the duplex from the closed ends, and they prevented complete dissociation of the construct if the duplex was fully melted. By having the two strands covalently linked, an experiment where the duplex was melted could be repeated for the same molecule several times. All constructs were pulled in a 3'-to-3' configuration, which means that the force is applied to the molecule by the 3'-ends of the opposite strands. Since the force was applied to the opposite strands, having an inter-strand linker also meant

that the length of a melted construct could be measured. Without a linker, complete separation of the strands in the double-stranded region results in breakage of the tether between the beads and the force drops to zero as the bead relaxes toward the center of the trap. The AT and GC sequences were also concatenated to form dimers (ATGC and GCGC) to study how sequence inhomogeneity and length effects influence the overstretching transition.

4.1.1 Building the constructs

The three core sequences were designed to have a GC-content of 60% (GC and GC2) or 30% (AT). They were also designed to be homogenous by adopting the criterion that the two halves of the sequences should have similar melting temperatures, as estimated by calculations of the nearest-neighbor energies [30]. Sequences of the specified GC-contents were randomly generated and the selection process was based on two criteria; the sequences should not form stable hairpins or self-complements. Unmodified oligonucleotides were purchased from IDT, US and oligonucleotides with modifications for inter-strand linkers were obtained from ATDBio, UK. Before hybridization of the synthesized oligonucleotide strands, the 3'-ends were extended using terminal transferase. Terminal deoxynucleotidyl transferase (TdT) is a polymerase that lacks 5'-to-3' exonuclease activity and can incorporate nucleotides without the requirement of a template strand. The nucleotide triphosphates that are available in the reaction mixture are added randomly to the 3'-end of the substrate oligonucleotide. The extension is performed to form single-stranded "handles" that can bind to the coated polystyrene beads used in the optical tweezers instrument. The TdT (New England Biolabs) reactions were performed using a dUTP-biotin/digoxigenin (Digoxigenin-11-dUTP, Biotin-16-dUTP, Roche) to dATP ratio of 1:10.
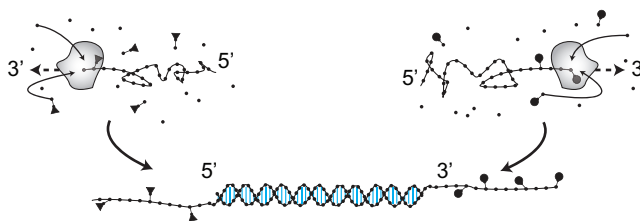

Figure 26 – Prior to hybridization of the two strands needed to form a duplex, each strand is extended using terminal transferase to incorporate biotin or digoxigenin labels.

The extension reactions were evaluated using polyacrylamide gel electrophoresis which showed that the length of each strand typically was increased by about 50 nucleotides. This elongation suggests incorporation of ~5 biotin or digoxigenin (DIG) modified uracil (U) nucleotides in the handles.

The variations of the GC and AT sequences designed to have inter-strand linkers were synthesized with alkyne and azide modified bases at either or both ends of the duplex region. After hybridization, the strands were covalently cross-linked using the CuAAC reaction (0.01eq oligonucleotide, 1eq CuSO4 • 5H2O, 7eq tris-hydroxypropyltriazole, 10eq Na ascorbate, overnight at 22 °C). The inter-strand links that were formed connect two C5-modified thymine bases on opposite strands diagonally from one modified base to the 5´-neighboring base on the complementary strand (see Figure 23). These bases were added to the core sequences and each site thus extends the double-stranded region by two AT base pairs. To maintain length consistency between single- and double-clicked versions of the constructs, two AT base pairs were also added to the other end of single-clicked constructs giving them a total duplex region of 64 base pairs. Figure 27 illustrates how the formed inter-strand linker protrudes into the major groove of the duplex as it connects the two strands.
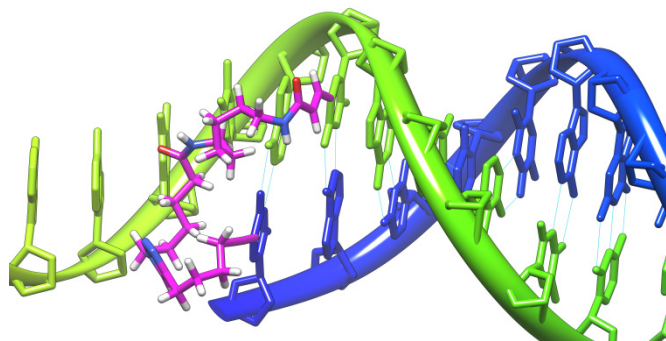
Figure 27 – The inter-strand "click-linker" (purple) connect two C5-modified thymine bases on opposite strands via the major groove.

4.1.2 Measuring the constructs

Measurements of the constructs were performed in a buffer environment (10 mM Tris pH 7.4, 1 mM EDTA) at room temperature (22-23 °C) either at high (1 M NaCl) or low (5 mM NaCl) salt concentration. The temperature was measured within the optical tweezers instrument close to the fluidics chamber. Glyoxal was used to study the potential occurrence of strand separation during overstretching in separate

experiments. In such exposure experiments, 0.5 M glyoxal (Sigma-Aldrich) was mixed in the buffer, and the pH was adjusted to 7.9. Streptavidin-coated polystyrene beads with a nominal diameter of 2.1 μm were used as obtained from Spherotech. AntiDIG-beads of the same size were prepared in-house by cross-linking anti-digoxigenin polyclonal antibodies (Roche) onto proteinG-modified polystyrene beads from Spherotech using Dimethyl pimelimidate (Sigma). The formation of a DNA-tether between the two beads was confirmed by gently pulling the construct, and the resulting force response was used to determine that the bridge only contained one DNA construct. Multiple tethers in parallel results in a force response that is stiffer than expected and a significantly increased overstretching force. Due to the curvature of the beads and the random distribution of labels on the ssDNA handles, events where several molecules bridge the two beads generally result in complex force spectrums as the different molecules have different extensions at a given force. Typically in this type of experiments, only the wanted case where a single DNA molecule connects the two beads gives reproducible results.

Once a tether containing a single DNA construct was established between the two beads, the standard stretching experiments were performed by moving the trap at a constant velocity (50 nm/s if not stated otherwise) to increase or reduce the force applied to the 3'-ends of the construct in a cyclic manner. Each cycle consisted of a stretching process where the force is increased from a lower force limit, F_{min}, to an upper force limit, F_{max}, and a relaxation process where the force is reduced from F_{max} back to F_{min} at the same rate. The force limits were set to ensure a hybridized B-form construct at the lower force limit and complete development of the studied overstretched states at the upper limit. The lowest force used was F_{min} = 15 pN and F_{max} was typically set to between 70 and 90 pN. One of the consequences of studying DNA constructs that have contour lengths of about 70-100 nm is that the relative stiffness is high compared to the rigidity of the optical trap, in this force region.

The change in force when moving the position of the trap can be described using an effective spring constant, κ_{eff}, for the system consisting of both the tethered DNA construct and the bead. Effectively the system acts as two springs in series, with one (non-linear) spring constant for the DNA, κ_{DNA}, and one for the trap, κ_{trap}. The measured force response is then related to the change in the position of the trap by $\kappa_{eff} = \left(\kappa_{DNA}^{-1} + \kappa_{trap}^{-1}\right)^{-1}$. Typically κ_{trap} is about 0.15-0.20 pN/nm which means that to generate a force of 10 pN the trap has to be displaced 50-67 nm from the center of the bead. For forces between F_{min} and F_{max} the stiffness of the DNA is dominated by the intrinsic elasticity ($K \sim 10^3$ pN) which means that for the

same change in force the constructs will only be extended by about 1 nm and that $\kappa_{eff} \approx \kappa_{trap}$. Commonly, the force response is represented by plots where the applied force is given as a function of the molecular extension. Such graphs are obtained by correcting for the compliance of the bead within the trap using the measured trap stiffness. For a molecule with a contour length of several μm, a small error in the determination of the trap stiffness will give an extension error that is small relative to the length of the molecule. However, as illustrated by the previous example, the same trap stiffness error would have a more significant effect for a short molecule. In this work, we plotted the force response as force versus trap position (in paper I, a change between two positions is referred to as distance) - which is the externally controlled parameter - to avoid introducing such errors. While force vs. extension plots arguably provide a more illustrative representation, both descriptions contain the same information regarding the transition [137].

A consequence of the fact that the position of the optical trap is controlled, combined with a relatively slow trap velocity, is that a sudden elongation of the construct is accompanied by a drop in the force as the bead relaxes toward the center of the trap. Contraction of the molecule consequently increases the force as the molecule pulls the bead away from the trap center. The change in length of the construct during such events can be measured by dividing the change in force by the stiffness of the system in the resulting state [137, 138]. During the experiments, measurement data was recorded a frequency of 1 kHz.

4.2   Overstretching GC-rich sequences

Figure 28 shows a force vs. trap position curve during a pull-relax cycle for a (non-clicked) 60 bp GC-construct in 1 M NaCl. The figure illustrates the typical behavior when the force is increased up to 70 pN and thereafter reduced. The molecule exhibits a force-dependent bistability as it oscillates between the B-form and an overstretched state. The inset in Figure 28A reveals how this switching back and forth between the two states occurs reversibly during both pulling and relaxation of the construct without any detectable hysteresis. Figure 28D shows a time trace of the measured force when the trap is stationary in the transition region. The oscillation of the molecule between B-form (high force) and the overstretched state (lower force) takes place on a millisecond time scale, and a histogram of the force data is well described by a double Gaussian fit. The bistability of the transition suggests that the overstretching can be understood in terms of a two-state process.

4.2.1 Analyzing reversible overstretching as a two-state process

The analysis was performed by assigning the force-position data points to either of the two states depending on their proximity to straight lines fitted at forces below and above the transition, respectively (see Figure 28B). The extent of the transition was then described by the probability of finding the system in the overstretched state P_S [139]. As the transition is observed as a change in force, the data was binned along the trap position axis and the occupancies of the two states were counted for each bin. Since the trap is moved at a constant velocity, this procedure is reduced to counting how many data points that correspond to each state N_S and N_B in the bin. Each pull or relax trajectory of a molecule is analyzed individually to minimize variations caused by instrument drift.

While the trap position provides a useable scale for the extent of the transition within a measurement, it is not directly applicable for comparison between molecules as the absolute position of the trap, the compliance of the bead within the trap, and the effective length of the constructs vary between different molecules. However, since the lines fitted to the data contain that information, they can be used to map the trap position onto a corresponding force which in turn can be used to describe the extent of the transition. Mapping of a position interval onto the force axis was performed in 0.5 pN intervals using the mean of the two fitted lines. The bins from all analyzed pull- and relax-curves were then pooled to determine the probabilities of each state as function of force. If we assume that the pulling and relaxation of the molecules is completely reversible, the probability of finding the molecule in a given state n can be presumed to follow the Boltzmann distribution.

$$P_n = \frac{g_n e^{-\Delta E_n/k_B T}}{\sum_n g_n e^{-\Delta E_n/k_B T}} = \frac{g_n e^{-(\Delta G - F\Delta x_n)/k_B T}}{\sum_n g_n e^{-(\Delta G - F\Delta x_n)/k_B T}} \tag{45}$$

For a system with two non-degenerate states B, and S, $(g_B = g_S = 1)$, the probabilities are given by

$$P_B = \frac{1}{1 + e^{-(\Delta G_{B\to S} - F\Delta x_{B\to S})/k_B T}}$$
$$P_S = \frac{e^{-(\Delta G_{B\to S} - F\Delta x_{B\to S})/k_B T}}{1 + e^{-(\Delta G_{B\to S} - F\Delta x_{B\to S})/k_B T}} \tag{46}$$

where $\Delta G_{B\to S}$ is the free energy difference between the two states at zero force, F the applied force, and $\Delta x_{B\to S}$ the cooperative change in length during the transition.
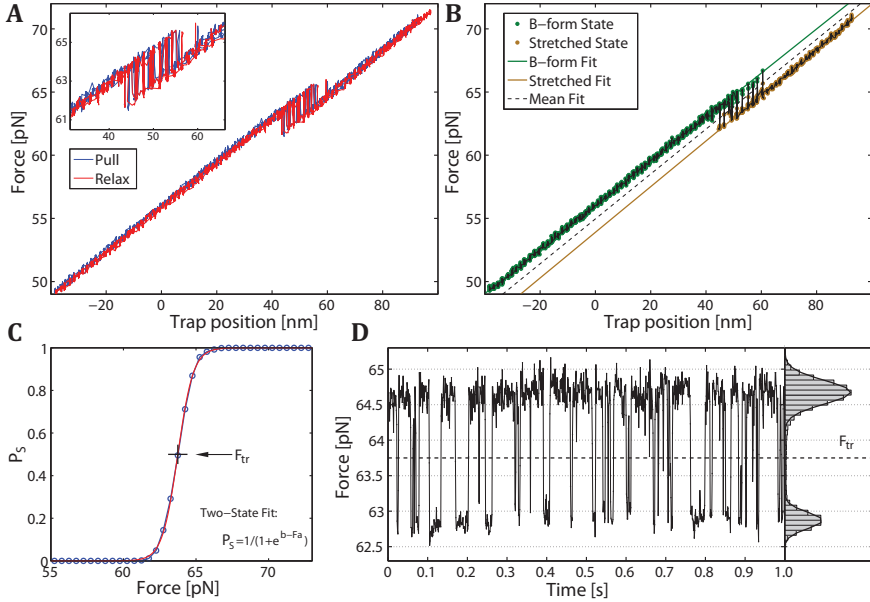
Figure 28 – Stretching of a single non-clicked 60 bp GC molecule (A) Force - Trap position plot during pulling (blue) and relaxation (red). The DNA duplex exhibits bistability between 61 and 65 pN, with no detectable hysteresis between the pulling and relaxation. (B) Force-position plot during a single pulling of the same molecule, illustrating the two-state analysis. Each data point is assigned to the B-form or the overstretched state depending on proximity to the lines fitted to the force-position data at low (green) and high force (brown), respectively. (C) The probability P_S of finding the molecule in the overstretched state as a function of force. Experimental data (circles) are pooled from 16 pull-and-relax cycles from the same molecule. (D) Time trace of the force in the overstretching region for the molecule measured at 1 kHz with the trap held stationary. The histogram (to the right) gives the distribution of the data points during the studied time interval (1s).

Using this model, the calculated probability of the overstretched state for each force interval was fitted as

$$P_S = \frac{N_S}{N_S + N_B} = \frac{1}{1 + e^{(b-Fa)/k_BT}} \tag{47}$$

where the two fit parameters a and b correspond to the cooperative length of the transition and the zero-force free energy difference, respectively. Equilibrium between the two states occur at $P_S = 0.5$, and the transition force F_{tr} defining that point is given by the fitted parameters as $F_{tr} = b/a$. The extension of the construct during the transition was then measured at F_{tr}, as the force difference between the

fitted lines divided by the slope of the resulting state, or equivalently as the position difference between the lines, since the slopes of the lines are constant.

4.2.2 Stretching the GC- and GC2-constructs in high salt

Figure 28C plots the probability of the overstretched state as a function of force obtained from 16 pull-relax cycles on the same GC molecule. The bistable behavior of the GC-constructs was also observed for the GC2-constructs when stretched in the same 1 M NaCl buffer. Based on data from 49 GC molecules, a mean transition force of F_{tr} = 63.3 ± 1.11 pN (± 1 s.d.) was obtained, and for GC2 (number of molecules, n = 33) F_{tr} = 62.0 ± 1.78 pN. The average extensions, measured at the transition force for each molecule, were 10.4 ± 0.46 nm for the GC-constructs and 11.2 ± 0.58 nm for the GC2-constructs. For a 60 bp duplex these numbers imply an average extension per base pair of 0.17 and 0.19 nm. These results reveal a stable form of DNA with a relative extension of only about 49 - 53%, which can be compared to previously observed extensions in longer sequences of about 70%.

By holding the trap stationary at different positions within the transition region, the kinetics of the bistable hopping between the two states can be measured. The lifetimes, τ, of the states are measured at each trap position by following how the molecule switches between them in the obtained time traces (see Figure 28D). To determine when a transition occurs, a partition force is introduced as the force half-way between the two peaks in the histogram of the time trace. The lifetime probability distributions are well described by a single exponential (not shown), which implies that the transition rates can be calculated as $k(F) = 1/\langle\tau\rangle$ [140]. Figure 29 show the natural logarithm of the transition rates as a function of the partition force for measurements performed on the same GC-molecule as in Figure 28. The intersection between the two fitted lines gives the equilibrium point where the extension and contraction of the molecule occur with the same rate. The results of this analysis show that the average lifetime (GC-construct, n=6) of the two states in this point is about 10.7 ± 2.7 ms.

The perhaps most important result from these experiments is that a double-stranded region of DNA that is only 60 bp long can be overstretched into a distinct extended state when stretched by the 3'-ends of the opposite strands. The stretched state was observed to be stable for up to minutes before dissociating. So what do the measurements tell us about the structure of the observed overstretched state in these molecules?
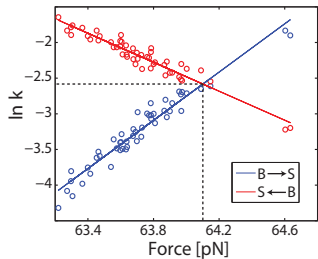
Figure 29 – Transition kinetics for the same GC-construct as in Figure 28. Each data point (circles) correspond to a 5 s sampling interval of the lifetimes. The natural logarithm of the transition rates are plotted against the partition force, and the equilibrium rate is given by the intersection between the linear fits to the data.

If we compare the extension of the constructs during the transition with the expected change in length for a peeling or internal melting process, we can calculate the number of base pairs that would remain in the overstretched state. The change in length is expected to be different for the two melting scenarios as the tension is divided differently between the two strands. In a peeling scenario, the tension would be supported by one strand, whereas in an internal melting case the tension would be shared between the molten strands (see Figure 30*i*. and *ii*.). An estimate of the expected length change can be obtained using the extensible worm-like chain (ExWLC, equation 40) and the freely jointed chain (ExFJC, equation 41) models. The number of base pairs that would remain paired upon melting can be assessed as

$$N_{ds} = N_{ds}^{tot} - \frac{\Delta x_{B-S}}{b_{ss}(F_{tr}, T) - b_{ds}(F_{tr}, T)}, \tag{48}$$

where N_{ds}^{tot} is the total number of base pairs in the duplex, $b_{ss}(F_{tr}, T)$ the rise per base in the resulting single strand (ExFJC) at the transition force, and $b_{ds}(F_{tr}, T)$ the rise per base pair of B-form DNA at the same force and temperature (ExWLC). The internal melting scenario was modeled with two parallel, noninteracting strands with a force response of $b_{2ss}(F) = b_{ss}(F/2)$ [107]. In this case, the analysis suggests that there would be no base pairs left to hold the two strands together, and is thus not a likely scenario. For a peeling scenario, the duplex would be left with 10-14 base pairs holding the two strands together. Such a duplex is however not expected to be stable at the temperature and ionic strength of the experiments while subjected to forces above F_{tr} [141, 142].
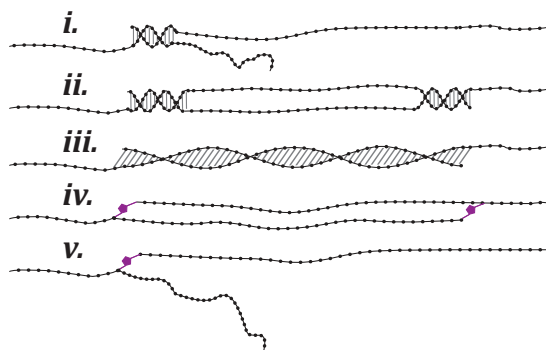
Figure 30 – Hypothetical overstretched states. (*i.*) Peeling of one strand off the other strand resulting in the tension only being supported by one of the released strands. (*ii.*) Melting occurs internally between two B-form regions. Here the tension is shared between the two formed single-strands. (*iii.*) S-form type of overstretching where the base-pairing remains intact during the extension. (*iv.*) Fully melted state of a double-clicked construct. (*v.*) Fully melted state of a single-clicked construct. A version of (*i.*) where only the inter-strand linker keeps the two strands from dissociating.

4.2.3 Clicked versions of the GC-construct compared to 5'AT

To further test the nature of the observed overstretched state, the click-sealed versions of the GC-construct (5'GC, 3'GC, and 3'5'GC) were studied using the same protocol as before in 1 M NaCl buffer. All three versions overstretched in a manner that was essentially indistinguishable when compared to the non-clicked GC-rich versions. Both the measured transition forces of 62-63 pN and the extensions per base pair of about 0.17-0.18 nm, were approximately the same as for the non-clicked constructs. The effect of the inter-strand linkers on the thermal stability of the constructs was assessed using denaturing polyacrylamide electrophoresis. The melting points of the duplex regions were estimated by running gels at temperatures ranging from 22°C to 74°C. As cross-linking is known to significantly increase the melting temperature [128], the experiments were performed with a urea concentration of 7 M in the gels to shift the melting to lower temperatures. Sealing one of the ends of the GC-construct increased the melting temperature by at least 20 degrees, and sealing both ends added another 10 degrees. These results confirm that the overstretching transition that is observed for the GC-rich duplexes is not related to thermal stability.

Complete strand separation occurs for GC-rich sequences. All stretching experiments come to an end in one way or another. The typical end point of an experiment is when the tether between the two beads is lost. For the non-clicked constructs this can be due to either complete melting of the duplex, or that the

handle on one or the other side unbinds from the bead. To distinguish between these possibilities is a difficult task. However, the introduction of the inter-strand linkers makes this distinction possible as complete strand separation then no longer leads to disruption of the tether between the beads (see Figure 30*iv.* and *v.*). Introducing an inter-strand linker also means that the length of the fully melted state can be measured, and that rehybridization can be studied.

Figure 31A shows the stretching of a 5'GC-construct in 1 M NaCl. In addition to the reversible overstretching, a second irreversible extension step is observed at a higher force. The second transition at ~74 pN extends the molecule by an additional 3.6 nm (see inset *ii.*) from the overstretched state and corresponds to complete melting of the duplex region (Figure 30*v.*). This melting results in hysteresis when the molecule is relaxed. The process is irreversible in the sense that the reverse transition back to the overstretched state does not occur. On the time scale of the experiments, rehybridization of the B-form does not occur until the force is reduced to about 20-25 pN. Experiments on the double-clicked 3'5'GC-construct supported the idea that cross-linking the ends inhibit melting as no constructs displayed any signs of melting even when exposed to forces up to 120 pN for extended periods of time.

Figure 31B shows Force vs. Trap position data for stretching of a 5'AT-construct in 1 M NaCl. The behavior of these constructs is different from that of the GC-constructs; instead of a reversible overstretching transition, the 5'AT-constructs undergo a distinct irreversible melting transition. Since the process is not reversible, another measure of transition force has to be defined. Instead of F_{tr}, a melting force F_m is defined as the highest force that is reached before the construct melts. The average melting force (n=16) for these constructs in 1 M NaCl was 61.5 ± 2.62 pN and resulted in an extension of the construct of 14.7 ± 0.99 nm (0.23 ± 0.02 nm/bp).

The measured extension agrees with the expected extension in a peeling process, as estimated using equation 48 (N_{ds} = -1 ± 4). As for the fully melted 5'GC-constructs rehybridization does not occur until the force is lowered to 20-25 pN. The large hysteresis of about 40 pN displayed by these fully melted single-clicked constructs is likely a result of the additional offset created by the inter-strand linker compared to a partially peeled state where neighboring base-paired bases may facilitate rehybridization. Figure 31B also shows (inset *i.*) that the stretched molecule exhibits bistability involving an intermediate state prior to the complete melting at F_m. This bistability was observed in most of the studied molecules and suggest that partial peeling of the duplex may be reversible on short length scales.
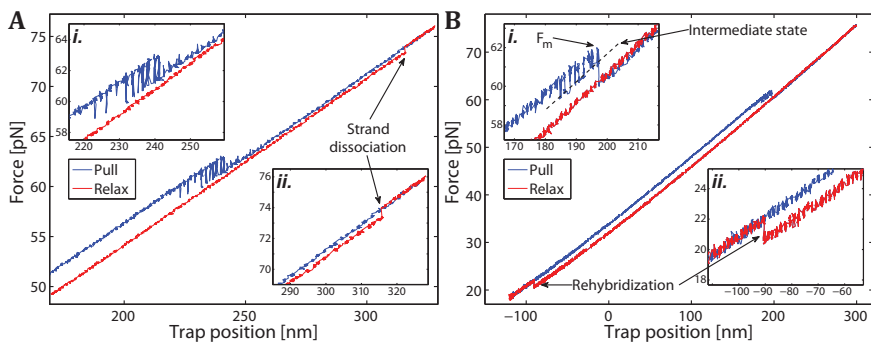
Figure 31 – Force vs. Trap position data for 5'GC- and 5'AT-constructs, both covalently sealed at one end (1 M NaCl). In both cases the main panel shows one cycle of pulling (blue) and relaxation (red) of a single DNA molecule. The insets show the details of the force-induced transitions that occur in the two different sequences. (A) 5′GC. During pulling reversible switching between two states is seen at about 60 pN. At 74 pN an abrupt decrease in force occurs during relaxation as the construct melts. (B) 5′AT. During pulling there is an abrupt transition to an extended state at 62 pN, and a significant hysteresis during the relaxation consistent with melting. Rehybridization to the B-form is observed as a return to the pulling curve at about 20 pN. Before the abrupt extension, at force F_m, reversible switching to a longer intermediate state is observed.

Measurements in 5 mM NaCl of the clicked versions of the GC-construct showed that a lower ionic strength lowers the stability toward melting. The 5'GC-construct displayed a behavior similar to that of the 5'AT-construct in 1 M NaCl, with an average melting force of 57.4 ± 1.45 pN (n=10). The double-clicked 3'5'GC-construct however still exhibited reversible overstretching without any signs of melting. The average transition force for the 3'5'GC-constructs was reduced slightly to 59.0 ± 0.52 pN (n=14), and so was the length of the transition which was reduced to 10.9 ± 0.61 nm. These results suggest that the type of overstretching is mainly determined by the stability of the sequence toward melting.

To investigate the degree of base-pairing in the two observed overstretched states, the 5'AT- (n=6) and the 3'5'GC-constructs (n=7) were exposed to 0.5 M glyoxal added to the high salt buffer. Figure 32A shows a 5'AT-construct before and after exposure to glyoxal while being held in the overstretched state. The results demonstrate that within a minute of exposure, the construct is significantly modified as seen by the reduced melting force during subsequent pull cycles.
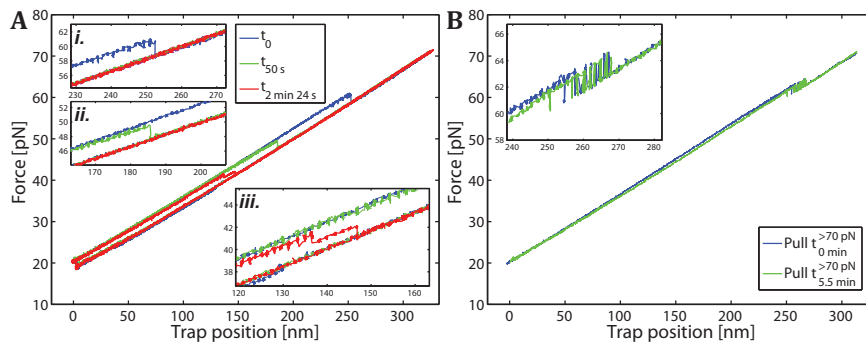
Figure 32 – Probing the overstretched states with glyoxal-reactivity. (A) 5´AT. The figure shows pull-relax cycles of a molecule in the presence of 0.5 M glyoxal. The blue curve is the first pull cycle before the molecule reacts and is modified by glyoxal and shows how it melts at about 60 pN (inset *i.*). After exposure of the melted molecule, the force is lowered to 20 pN to allow for rehybridization. The green curve shows the same molecule after it has been exposed in the melted state to glyoxal for a total of 50s. The molecule is seen to melt at about 49 pN (inset *ii.*). The red curve shows the molecule after a total exposure time of 2 min and 24 s. Here the molecule first partially melts before it completes the melting at 41 pN (inset *iii.*). (B) 3´5´GC. The blue curve shows the first pull of the molecule in the presence of glyoxal, while the green curve shows a pull of the same molecule after 5 min 30 s of exposure to the agent while in the overstretched state (>70 pN). The depicted curves have been horizontally compensated for instrument drift (<4 nm/min).

Figure 32B shows a 3'5'GC-construct before and after exposure. Even though the molecule is held in the overstretched state for a total of 5.5 minutes, no significant change can be observed. These results confirm that the irreversible transition observed for the 5'AT-constructs indeed is a melting transition. The results also show that the bases in the reversible overstretched state of the GC-constructs are not accessible to reaction with glyoxal.

The presented results reveal that the AT-rich 5'AT-construct undergoes a force-induced melting transition, leaving it in a state where the base-pairing between the two strands is completely disrupted (see Figure 30*v.*). In contrast to this behavior, the results also suggest that the GC-rich constructs retain the base-pairing during overstretching in high salt - as was originally suggested for S-form DNA (see Figure 30*iii.*) – and that this form of DNA appears to be shorter than expected.

4.3   Force-induced melting of AT-rich constructs

Figure 33 shows high salt (1 M NaCl) stretching results of the double-clicked 3'5'AT-construct. Overstretching of the molecule occurs gradually over a force interval between 60 pN and 70 pN (Figure 33A). This behavior is distinctly different compared to the transitions observed for the single-clicked 5'AT-construct and the GC-rich sequences, as it displays no discernible intermediates. Relaxation of the molecules is observed to follow two different trajectories; one non-hysteretic where the trajectory follows the pull-curve as the force is reduced, and one hysteretic rehybridization behavior shown in Figure 33C. About half of the studied 3'5'AT molecules (15 out of 31) displayed one or more hysteretic relaxation trajectories. However, both relaxation pathways are available to a given 3'5'AT molecule as the two behaviors could be observed in one and the same molecule. Figure 33D shows stretching of a 3'5'AT molecule in the presence of 0.5 M glyoxal. The results show that the molecule becomes significantly modified when exposed to glyoxal in the fully extended state, which together with the hysteretic rehybridization behavior suggest that the 3'5'AT-construct melts under tension. Since the peeling mechanism is inhibited by the covalent seals in both ends of the construct, the melting is likely to be initiated internally in the duplex as illustrated in Figure 30*ii*.

The gradual nature of the transition suggests a low degree of cooperativity compared to the abrupt melting of the 5'AT-construct and the B-to-S-form transition of the GC-rich sequences. To determine F_{tr} for the transition, the previously described two-state analysis had to be modified, and the extent of the reaction was instead described as the relative distance of each data point to linear fits of the data below and above the transition region. The resulting fits to this adapted two-state model (see Figure 33B) resulted in a mean value for F_{tr} of 67.8 ± 1.01 pN (n=31). The mean extension at F_{tr} was measured to be 10.6 ± 1.26 nm (0.17 ± 0.02 nm/bp). These data suggest that internal melting of a given sequence occurs at higher forces than peeling of the same, and results in shorter extension of the molecule during the transition.

The experiments also raise an interesting question regarding sequence dependence of the overstretching transition. One might have expected that the result of sealing both end of the duplex would be a B-to-S-form transition as in the GC-rich constructs under the same conditions. However, the data show no signs that such a process would precede the melting, indicating that the S-form perhaps is not accessible for all sequences.
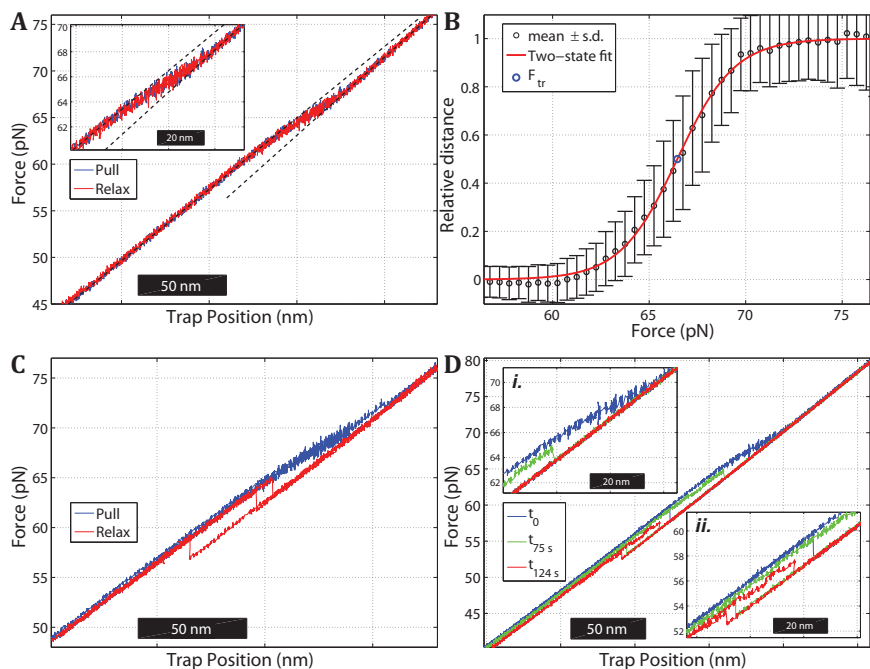
Figure 33 – Stretching of a double-clicked 3'5'AT-construct in 1 M NaCl.(A) Plot of force vs. trap position during one cycle of pulling (blue) and relaxation (red). The DNA duplex exhibits a continuous reversible transition over a broad force interval (60-70 pN). Dashed lines show linear fits to the data below and above the transition region used to define the two end states. (B) Pooled data from 9 pull and relax cycles of the same molecule showing the relative extension of the duplex as a function of force. Experimental data (circles with error bars ± 1. s.d.) and a fit to a two-state model (red curve) to estimate F_{tr}. (C) Multiple pull- and relax trajectories of a 3'5'AT molecule exhibiting hysteresis during the relaxation. (D) Pull experiments on a 3'5'AT molecule in the presence of 0.5 M glyoxal (1 M NaCl, pH 7.9) before and after reaction. The blue curve is the pulling trace before the DNA was exposed to glyoxal. The molecule was then held at 74 pN to expose the stretched construct to the glyoxal. The green and red curves show the pull-relax traces of the same molecule after a total exposure time in the fully stretched state of 75 and 124 seconds, respectively. The transition force is reduced to about 65 pN (green curve in inset *i.*) and 57 pN (red curve in inset *ii.*), respectively, indicating the formation of glyoxal adducts.

An alternative explanation is that the DNA first extends into S-form which then quickly melts on a time scale faster than what we are capable of measuring. Regardless of the mechanism, the experiments suggest that all three of the proposed modes of overstretching can be found in short DNA-constructs.

Stretching of the 3'5'AT-constructs in 5 mM NaCl alters the behavior of the transition. Instead of the gradual transition observed at high salt the duplex melts in a single discrete step, similar to the melting behavior of the single-clicked construct. The average melting force (n=14) for the constructs was 61.0 ± 2.27 pN, which can be compared with the value for the single-clicked 5'AT-constructs of 43.6 ± 2.79 pN (n=12) under the same conditions. During relaxation in 5 mM NaCl, both the 3'5'AT- and the 5'AT-constructs exhibit hysteresis and rehybridize in a single step. However, the average force at which the rehybridization occurs differs significantly between the two. While the single-clicked 5'AT-construct rehybridizes at an average force of 17.3 ± 0.98 pN, the double-clicked 3'5'AT-construct does the same at 41.1 ± 4.88 pN. The higher rehybridization force for the 3'5'AT-constructs is likely a result of the two strands having similar extensions and being kept close to each other by the inter-strand linkers, both of which should increase the rate of rehybridization. The significant impact that the ionic strength has on the force-induced melting of these short DNA constructs confirm results observed for long heterogeneous DNA [51].

4.4 Stretching "dimers"

Figure 34 show overstretching results of the ATGC-construct under various conditions. The construct is a "dimer" of the AT-rich and GC-rich sequences created with the purpose of studying how the two known parts of the constructs interact during overstretching. The distinct heterogeneity of the construct sequence was also expected to provide a duplex end point for the potential melting of the AT-rich region, as the GC-rich part was expected to retain its base-pairing at such forces.

Figure 34A shows multiple pull and relax cycles of an ATGC-molecule in 1 M NaCl. The curves exhibit two bistable reversible transitions (a. and b.), suggesting that the behavior could be described by extending the previous two-state model into a three-state model to include an intermediate state I. Figure 34B presents the three-state probability analysis for the same molecule, and shows that the three states are well separated in force. The transition force F_{tr} for the overall process was defined as the maximum in the fitted population of the intermediate state, and resulted in an average value of 64.3 ± 0.8 pN (n=8) accompanied by a total extension of 24.7 ± 1.0 nm (0.20 nm/bp). To investigate the degree of base-pairing in the fully stretched state, the ATGC-constructs were also stretched with glyoxal present in the high salt buffer. Figure 34D presents the results of such an experiment, and reveals how the first transition (a.) is modified during exposure to glyoxal while the second transition (b.) remains unaffected.
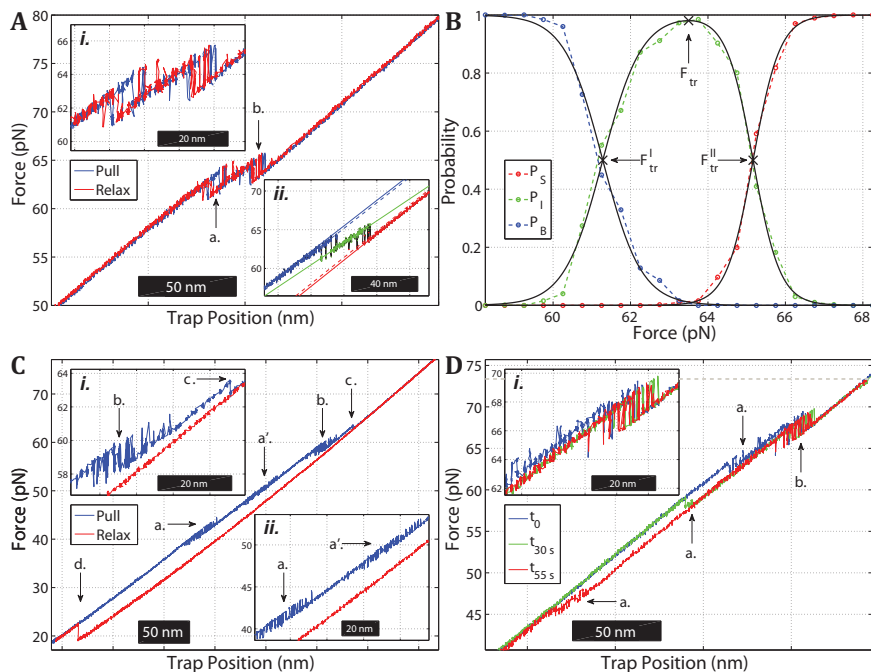
Figure 34 – Force-induced melting and rehybridization of the ATGC construct. (A) Force vs. trap position trajectories during multiple pull-relax cycles on an ATGC molecule in 1 M NaCl. The two distinct transitions (a. & b.) are reversible. Inset *i.* shows that the two transitions are well separated in force and that both exhibit bistability. Inset *ii.* shows a single pull trajectory for the same molecule and the linear fits (dashed) used to assign the data points to the three states at low (blue), intermediate (green) and high force (red). (B) Population probabilities of the three states as a function of force for the molecule in (A), based on pooled data from pull and relax trajectories. The fitted curves (black) are used to estimate the transition forces F_{tr}^{I}, F_{tr} and F_{tr}^{II}. (C) Force vs. trap position trajectory during a pull-relax cycle on an ATGC molecule in 5 mM NaCl. During pulling (blue) ATGC exhibits four transitions (a. - c.) The first three transitions display bistability (a. and a'. in inset *ii.*, b. in inset *i.*) while the fourth transition is irreversible (c. in inset *i.*). During relaxation (red) the molecule rehybridizes at about 20 pN (d.). (D) Pull trajectories of an ATGC molecule in the presence of 0.5 M glyoxal (1 M NaCl, pH 7.9) before (t_0; blue) and after glyoxal reaction for 30s (t_{30s}; green) and 55s (t_{55s}; red) in the fully extended state (gray dotted line). The first transition (a.). at about 65 pN (see also a. in panel A) occurs at lower forces after glyoxal exposure, at 58 pN after 30s and at 47 pN after 55s, respectively.

When comparing with exposure experiments performed on the two parts of the dimer (Figure 32), these results suggest that the first transition (a.) corresponds to the melting of the AT-rich part while the second transition (b.) is the B-to-S-form overstretching of the GC-rich half of the construct. This interpretation is supported

by the results of the low salt stretching of the construct plotted in Figure 34C. The first transition (a.) is significantly affected by the change in ionic strength while the transition force of the second (b.) is reduced by only a few pN. The figure also shows how the first transition (a.), corresponding to peeling of the AT-rich part, is followed by another transition (a'.) before the B-to-S-form transition (b.) of the GC-rich part. Inspection of the intermediate state, I, in the high salt experiments show that the slope of the lines fitted to the state (Figure 34A, inset *ii.*) is shallower than those of the B and S states, indicating that the construct is extended within the intermediate state. Close inspection of the glyoxal experiment (Figure 34D, inset *i.*) also reveal that the intermediate state is modified during exposure. These results suggest that the peeling of the AT-rich part of the construct occurs in two steps, where the most distal regions peel first and the region proximal to the GC-rich sequence melts in a second step. This behavior suggests that proximity to a neighboring base-paired region increases the equilibrium melting force, likely due to an increased rehybridization rate. An important conclusion that can be drawn from the ATGC and 3'5'AT experiments is that while hysteresis is a sign of melting, the lack of it does not necessarily mean that no melting occurs.

Figure 35 shows an example of a GCGC-dimer that is stretched in 1 M NaCl. The molecule displays a reversible overstretching transition that is not as resolved as in the ATGC-dimer, but shows signs of at least one intermediate state. The results using the same type of three-state analysis as for the ATGC-constructs give an average transition force F_{tr} of 64.3 ± 1.56 pN (n=17) and a total extension during the transition of 23.8 ± 1.93 nm (0.195 ± 0.016 nm/bp).
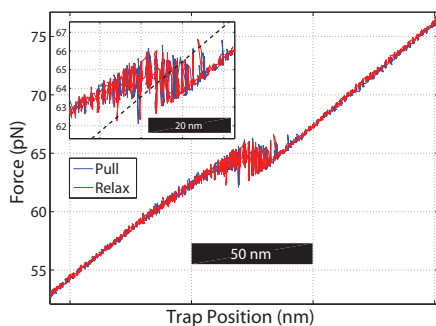
Figure 35 – Force vs. Trap position plot showing a single pull and relax cycle of a GCGC-construct in 1 M NaCl. The observed transition is reversible but more complex compared to the transition seen for the different versions of the GC-constructs, suggesting that there is one or more intermediates formed during the process.

In conclusion, the results from the two dimer-constructs show that concatenating sequences with known properties in a "bottom-up" fashion provides a useful approach to studying the DNA overstretching transition. The complexity of the observed transition increases with the increasing size of the system, but the results confirm that the whole is not greater than the sum of its parts.

5 Concluding remarks

The work presented in this thesis show how the overstretching transition of torsionally unconstrained double-stranded DNA can be studied for short DNA-sequences. By reducing the length of the studied DNA, it was proven that it is possible to isolate and study, in an independent fashion, the different processes that can occur during the overstretching transition. Using this approach we could confirm that all three mechanisms that have been proposed over the years can indeed be observed during overstretching under the appropriate conditions.

The results show that overstretching into a longer but still base-paired form of DNA, commonly referred to as S-form DNA, is possible for GC-rich sequences. Under the right experimental conditions, such as high ionic strength, this form of DNA can remain stable for extended periods of time. Furthermore, these sequences can extend into S-form also at low ionic strengths, but quickly thereafter they melt if the strand-separation process is not inhibited. Force-induced melting on the other hand, is favoured for AT-rich sequences under both high and low salt conditions. It was also found that distinguishing between force-induced melting and B-to-S-form transitions can be difficult, even for short well defined sequences. The work presented in this thesis together with other recent reports in the field [143, 144] have helped resolve some of the seemingly conflicting observations of the DNA overstretching transition, but it is still far from fully understood.

There exists no accurate way of predicting exactly how a certain sequence will overstretch under given experimental conditions and the kinetics of the processes are only poorly understood. Even the resulting extensions during the different modes of overstretching cannot be considered as completely defined. While the extension resulting from a peeling process is fairly well known, the extension during internal melting is typically only estimated by assuming that the two strands do not interact with each other and share the tension evenly. To truly test those assumptions, the complete behavior of the overstretched sequence must be known. The presented work takes a step in that direction by isolating the process. However, the same lack of averaging that means that the process can be isolated in a short sequence, also makes it difficult to determine the absolute extension and sequence dependence of the process. The principle of concatenating sequences with a known behavior can indeed be applied when making longer DNA than the sequences used in this work, which would resolve these issues.

The double-stranded regions of the dimer-constructs studied in this work are completely synthetic which limits their lengths to a couple of hundred base pairs, but by using enzymatic techniques the length range of concatenated constructs can be extended into thousands of base pairs. By flanking a long homogenous AT-rich region with highly GC-rich ends, the process of internal melting could be studied in an almost completely isolated form. The same approach could also be used to build constructs designed to study the properties of the B-to-S-form transition. The challenge lies in avoiding all the potential unwanted side effects that can come from concatenating identical sequences. For example, a GCGC-construct eventually melts when stretched in low salt, and the two identical regions of the constructs allows it to rehybridize in a mismatched configuration that is stable at room temperature. This mismatched configuration corresponds to the complementary region of the second half of the construct hybridizing with the first half and is just one example of such "unwanted" effects that come with building a longer more complex construct. Solving such issues would however yield a molecule suitable for studying how different ligands interact with S-form DNA, which could answer the question of what the structure of the DNA is in this state. Isolating the B-to-S transition is also a necessity when it comes to understanding what the biological relevance of such a base-paired stretched state may be. The constructs studied here have all been stretched 3'-to-3', but by modifying the attachment strategy 5'-to-5' and 5'-to-3' stretching could be performed. Doing so will likely provide an enhanced understanding of how the modes of overstretching are related to how the force is applied.

In conclusion, many unresolved issues remain, and much effort needs to be invested before a complete comprehension of the DNA overstretching process can be achieved. Hopefully, the findings presented in this thesis can provide a good point of departure for prospective investigators aiming at increasing our knowledge about the DNA overstretching transition and its biological implications.

6 Acknowledgements

I would like to express my gratitude and appreciation to all the people that have supported and helped me over the years. Without you, this would not have been possible. I would especially like to thank:

Bengt - for giving me the opportunity to do this work and for giving me the freedom to pursue my ideas. Growing up, I played a lot with Lego®, and to be allowed to build an instrument has given me more of that childhood fun.

Björn - for …well, most things really. You got me interested in and taught me physical chemistry, but most of all I would like to thank you for always finding time for me. I have truly enjoyed working with you.

Steve - for introducing me to optical tweezers and showing me how to use them. The three months that I spent working with you in Berkeley were enormously inspirational.

My other co-authors: Tom Brown, Carlos Bustamante, and Afaf El-Sagheer - for your time and efforts.

Nils, Lena, and Maria have my deepest gratitude for taking the time to proofread this thesis.

Helene, Karolin, and Elin – for being great room company and for delivering fantastic pep talks.

Past and present colleagues at Physical Chemistry – for creating an enjoyable working environment.

My family – for supporting and believing in me. I am especially grateful to my mom Ann; all your help during the writing of this thesis has been invaluable (and you know… for everything else as well).

Marja and Ingrid, you are my life and the joy that fills it, I love you so much.

7 References

1. Chen, Z., H. Yang, and N.P. Pavletich, *Mechanism of homologous recombination from the RecA-ssDNA/dsDNA structures.* Nature, 2008. **453**(7194): p. 489-494.

2. Killian, J.L., et al., *Recent advances in single molecule studies of nucleosomes.* Current Opinion in Structural Biology, 2012. **22**(1): p. 80-87.

3. Dame, R.T., M.C. Noom, and G.J.L. Wuite, *Bacterial chromatin organization by H-NS protein unravelled using dual DNA manipulation.* Nature, 2006. **444**(7117): p. 387-390.

4. Bustamante, C., *In singulo biochemistry: When less is more.* Annual Review of Biochemistry, 2008. **77**(1): p. 45-50.

5. Ashkin, A., *Acceleration and trapping of particles by radiation pressure.* Physical Review Letters, 1970. **24**(4): p. 156.

6. Ashkin, A., *Trapping of atoms by resonance radiation pressure.* Physical Review Letters, 1978. **40**(12): p. 729-732.

7. Ashkin, A., et al., *Observation of a single-beam gradient force optical trap for dielectric particles.* Opt. Lett., 1986. **11**(5): p. 288.

8. Svoboda, K. and S.M. Block, *Biological applications of optical forces.* Annual Review of Biophysics and Biomolecular Structure, 1994. **23**(1): p. 247-285.

9. Chu, S., et al., *Experimental observation of optically trapped atoms.* Physical Review Letters, 1986. **57**(3): p. 314-317.

10. Chu, S., *Laser manipulation of atoms and particles.* Science, 1991. **253**(5022): p. 861-866.

11. Chu, S., *1997 Nobel lecture in physics: The manipulation of neutral particles*, in *Nobel Lectures, Physics 1996-2000*, G. Ekspong, Editor. 2002, World Scientific Publishing Co.: Singapore. p. 122-158.

12. Ashkin, A. and J. Dziedzic, *Optical trapping and manipulation of viruses and bacteria.* Science, 1987. **235**(4795): p. 1517-1520.

13. Ashkin, A. and J.M. Dziedzic, *Internal cell manipulation using infrared laser traps.* Proceedings of the National Academy of Sciences, 1989. **86**(20): p. 7914-7918.

14. Ashkin, A., J.M. Dziedzic, and T. Yamane, *Optical trapping and manipulation of single cells using infrared laser beams.* Nature, 1987. **330**(6150): p. 769-771.

15. Block, S.M., D.F. Blair, and H.C. Berg, *Compliance of bacterial flagella measured with optical tweezers.* Nature, 1989. **338**(6215): p. 514-518.

16. Wright, W.H., et al., *Laser trapping in cell biology.* IEEE Journal of Quantum Electronics, 1990. **26**(12): p. 2148-2157.

17.   Moffitt, J.R., et al., *Recent advances in optical tweezers*. Annual Review of Biochemistry, 2008. **77**(1): p. 205-228.

18.   Smith, S.B., Y. Cui, and C. Bustamante, *Optical-trap force transducer that operates by direct measurement of light momentum*. Methods in Enzymology, 2003. **361**: p. 134-160.

19.   Bustamante, C. and S.B. Smith, *Optical beam translation device and method using a pivoting optical fiber*, in *United States Patent* 2007: United States.

20.   Bustamante, C. and S.B. Smith, *Light-Force sensor and method for measuring axial optical-trap forces from changes in light momentum along an optical axis.*, in *United States Patent* 2006: United States.

21.   Wilson, K. and J. Walker, eds. *Principles and techniques of biochemistry and molecular biology*. 6:th ed. 2005, Cambridge University Press.

22.   Portugal, F.H. and J.S. Cohen, *A century of DNA*. 1979: MIT Press.

23.   Griffith, F., *The significance of pneumococcal types*. Epidemiology & Infection, 1928. **27**(02): p. 113-159.

24.   Avery, O.T., C.M. MacLeod, and M. McCarty, *Studies on the chemical nature of the substance inducing transformation of pneumococcal types: induction of transformation by a desoxyribonucleic acid fraction isolated from pneumococcus type III*. The Journal of Experimental Medicine, 1944. **79**(2): p. 137-158.

25.   Chargaff, E., et al., *The composition of the desoxyribonucleic acid of salmon sperm*. Journal of Biological Chemistry, 1951. **192**(1): p. 223-230.

26.   Watson, J.D. and F.H.C. Crick, *Molecular structure of nucleic acids: A structure for deoxyribose nucleic acid*. Nature, 1953. **171**(4356): p. 737-738.

27.   Watson, J.D. and F.H.C. Crick, *Genetical implications of the structure of deoxyribonucleic acid*. Nature, 1953. **171**(4361): p. 964-967.

28.   Franklin, R.E. and R.G. Gosling, *Molecular configuration in sodium thymonucleate*. Nature, 1953. **171**(4356): p. 740-741.

29.   Wilkins, M.H.F., A.R. Stokes, and H.R. Wilson, *Molecular structure of nucleic acids: Molecular structure of deoxypentose nucleic acids*. Nature, 1953. **171**(4356): p. 738-740.

30.   SantaLucia, J., *A unified view of polymer, dumbbell, and oligonucleotide DNA nearest-neighbor thermodynamics*. Proceedings of the National Academy of Sciences, 1998. **95**(4): p. 1460-1465.

31.   Franklin, R.E. and R.G. Gosling, *Evidence for 2-chain helix in crystalline structure of sodium deoxyribonucleate*. Nature, 1953. **172**(4369): p. 156-157.

32.   Kresge, N., R.D. Simoni, and R.L. Hill, *The discovery of Z-DNA: the work of Alexander Rich*. Journal of Biological Chemistry, 2009. **284**(51): p. e23-e25.

33.   Wang, A.H.J., et al., *Molecular structure of a left-handed double helical DNA fragment at atomic resolution.* Nature, 1979. **282**(5740): p. 680-686.

34.   Reymer, A., *Unveiling mechanistic details of macromolecular interactions: Structural design and molecular modelling of DNA-protein systems in their active state*, in *Department of Chemical and Biological Engineering* 2012, Chalmers University of Technology.

35.   Kuhn, W. and F. Grün, *Beziehungen zwischen elastischen konstanten und dehnungsdoppelbrechnung hochelastischer stoffe.* Kolloid-Zeitschrift, 1942. **101**(3): p. 248-271.

36.   Cantor, C.R. and P.R. Schimmel, *Biophysical chemistry part III: The behavior of biological macromolecules.* 1980: W. H. Freeman and Company.

37.   Hiromi, Y., *Modern theory of polymer solutions.* Harper's chemistry series. 1971: Harper & Row.

38.   Kratky, O. and G. Porod, *Röntgenuntersuchung gelöster fadenmoleküle.* Recueil des Travaux Chimiques des Pays-Bas, 1949. **68**(12): p. 1106-1122.

39.   Doi, M. and S.F. Edwards, *The theory of polymer dynamics.* 1986: Oxford University Press.

40.   Hagerman, P.J., *Flexibility of DNA.* Annual Review of Biophysics and Biophysical Chemistry, 1988. **17**(1): p. 265-286.

41.   Bloomfield, V.A., D.M. Crothers, and I. Tinoco, *Nucleic acids: structures, properties, and functions.* 2000, Sausalito, CA: University Science Books.

42.   Marko, J.F. and E.D. Siggia, *Stretching DNA.* Macromolecules, 1995. **28**(26): p. 8759-8770.

43.   Odijk, T., *Stiff chains and filaments under tension.* Macromolecules, 1995. **28**(20): p. 7016-7018.

44.   Smith, S.B., L. Finzi, and C. Bustamante, *Direct mechanical measurements of the elasticity of single DNA molecules by using magnetic beads.* Science, 1992. **258**(5085): p. 1122-1126.

45.   Smith, S.B., Y. Cui, and C. Bustamante, *Overstretching B-DNA: The elastic response of individual double-stranded and single-stranded DNA molecules.* Science, 1996. **271**(5250): p. 795-799.

46.   Manning, G.S., *Limiting laws and counterion condensation in polyelectrolyte solutions I. Colligative properties.* The Journal of Chemical Physics, 1969. **51**(3): p. 924-933.

47.   Manning, G.S., *Counterion binding in polyelectrolyte theory.* Accounts of Chemical Research, 1979. **12**(12): p. 443-449.

48.   Odijk, T., *Polyelectrolytes near the rod limit.* Journal of Polymer Science: Polymer Physics Edition, 1977. **15**(3): p. 477-483.

49. Skolnick, J. and M. Fixman, *Electrostatic persistence length of a wormlike polyelectrolyte.* Macromolecules, 1977. **10**(5): p. 944-948.

50. Baumann, C.G., et al., *Ionic effects on the elasticity of single DNA molecules.* Proceedings of the National Academy of Sciences, 1997. **94**(12): p. 6185-6190.

51. Wenner, J.R., et al., *Salt dependence of the elasticity and overstretching transition of single DNA molecules.* Biophysical Journal, 2002. **82**(6): p. 3160-3169.

52. Bustamante, C., et al., *Single-molecule studies of DNA mechanics.* Current Opinion in Structural Biology, 2000. **10**(3): p. 279-285.

53. Wang, M.D., et al., *Stretching DNA with optical tweezers.* Biophysical Journal, 1997. **72**(3): p. 1335-1346.

54. Podgornik, R., P.L. Hansen, and V.A. Parsegian, *Elastic moduli renormalization in self-interacting stretchable polyelectrolytes.* The Journal of Chemical Physics, 2000. **113**(20): p. 9343-9350.

55. Bouchiat, C., et al., *Estimating the persistence length of a worm-like chain molecule from force-extension measurements.* Biophysical Journal, 1999. **76**(1): p. 409-413.

56. Cloutier, T.E. and J. Widom, *DNA twisting flexibility and the formation of sharply looped protein–DNA complexes.* Proceedings of the National Academy of Sciences, 2005. **102**(10): p. 3645-3650.

57. Wiggins, P.A., et al., *High flexibility of DNA on short length scales probed by atomic force microscopy.* Nature Nanotechnology, 2006. **1**(2): p. 137-141.

58. Vafabakhsh, R. and T. Ha, *Extreme bendability of DNA less than 100 base pairs long revealed by single-molecule cyclization.* Science, 2012. **337**(6098): p. 1097-1101.

59. Du, Q., et al., *Cyclization of short DNA fragments and bending fluctuations of the double helix.* Proceedings of the National Academy of Sciences, 2005. **102**(15): p. 5397-5402.

60. Yan, J. and J.F. Marko, *Localized single-stranded bubble mechanism for cyclization of short double helix DNA.* Physical Review Letters, 2004. **93**(10): p. 108108.

61. Wiggins, P.A. and P.C. Nelson, *Generalized theory of semiflexible polymers.* Physical Review E, 2006. **73**(3): p. 031906.

62. Crick, F.H.C. and A. Klug, *Kinky helix.* Nature, 1975. **255**(5509): p. 530-533.

63. Vologodskii, A. and M. D. Frank-Kamenetskii, *Strong bending of the DNA double helix.* Nucleic Acids Research, 2013.

64. Wilkins, M.H.F., R.G. Gosling, and W.E. Seeds, *Physical studies of nucleic acid: Nucleic acid: an extensible molecule?* Nature, 1951. **167**(4254): p. 759-760.

65. Kishino, A. and T. Yanagida, *Force measurements by micromanipulation of a single actin filament by glass needles.* Nature, 1988. **334**(6177): p. 74-76.

66. Binnig, G., C.F. Quate, and C. Gerber, *Atomic force microscope.* Physical Review Letters, 1986. **56**(9): p. 930-933.

67. Smith, S.B., P.K. Aldridge, and J.B. Callis, *Observation of individual DNA molecules undergoing gel electrophoresis.* Science, 1989. **243**(4888): p. 203-206.

68. Moerner, W.E. and L. Kador, *Optical detection and spectroscopy of single molecules in a solid.* Physical Review Letters, 1989. **62**(21): p. 2535-2538.

69. Morikawa, K. and M. Yanagida, *Visualization of individual DNA molecules in solution by light microscopy: DAPI staining method.* The Journal of Biochemistry, 1981. **89**(2): p. 693-696.

70. Orrit, M. and J. Bernard, *Single pentacene molecules detected by fluorescence excitation in a p-terphenyl crystal.* Physical Review Letters, 1990. **65**(21): p. 2716-2719.

71. Brooks Shera, E., et al., *Detection of single fluorescent molecules.* Chemical Physics Letters, 1990. **174**(6): p. 553-557.

72. Parra, I. and B. Windle, *High resolution visual mapping of stretched DNA by fluorescent hybridization.* Nature Genetics, 1993. **5**: p. 17-21.

73. Bensimon, D., et al., *Stretching DNA with a receding meniscus: Experiments and models.* Physical Review Letters, 1995. **74**(23): p. 4754-4757.

74. Thundat, T., D.P. Allison, and R.J. Warmack, *Stretched DNA structures observed with atomic force microscopy.* Nucleic Acids Research, 1994. **22**(20): p. 4224-4228.

75. Perkins, T.T., et al., *Relaxation of a single DNA molecule observed by optical microscopy.* Science, 1994. **264**(5160): p. 822-826.

76. Perkins, T.T., D.E. Smith, and S. Chu, *Direct observation of tube-like motion of a single polymer chain.* Science, 1994. **264**(5160): p. 819-822.

77. Bustamante, C., et al., *Entropic elasticity of λ-phage DNA.* Science, 1994. **265**(5178): p. 1599-1600.

78. Smith, S.B., et al., *Stretching DNA beyond its B-form contour length.* Biophysical Journal, 1995. **68**: p. A250.

79. Cluzel, P., et al., *DNA: An extensible molecule.* Science, 1996. **271**(5250): p. 792-794.

80. Cizeau, P. and J.-L. Viovy, *Modeling extreme extension of DNA.* Biopolymers, 1997. **42**(4): p. 383-385.

81. Ahsan, A., J. Rudnick, and R. Bruinsma, *Elasticity Theory of the B-DNA to S-DNA Transition.* Biophysical Journal, 1998. **74**(1): p. 132-137.

82. Lebrun, A. and R. Lavery, *Modelling extreme stretching of DNA.* Nucleic Acids Research, 1996. **24**(12): p. 2260-2267.

83. Konrad, M.W. and J.I. Bolonick, *Molecular dynamics simulation of DNA stretching is consistent with the tension observed for extension and strand separation and*

predicts a novel ladder structure. Journal of the American Chemical Society, 1996. **118**(45): p. 10989-10994.

84. Kosikov, K.M., et al., *DNA stretching and compression: large-scale simulations of double helical structures.* Journal of Molecular Biology, 1999. **289**(5): p. 1301-1326.

85. Rief, M., H. Clausen-Schaumann, and H.E. Gaub, *Sequence-dependent mechanics of single DNA molecules.* Nature Structural Biology, 1999. **6**(4): p. 346 - 349.

86. Clausen-Schaumann, H., et al., *Mechanical stability of single DNA molecules.* Biophysical Journal, 2000. **78**(4): p. 1997-2007.

87. Hogan, M.E. and R.H. Austin, *Importance of DNA stiffness in protein-DNA binding specificity.* Nature, 1987. **329**(6136): p. 263-266.

88. Lee, G.U., L.A. Chrisey, and R.J. Colton, *Direct measurement of the forces between complementary strands of DNA.* Science, 1994. **266**(5186): p. 771-773.

89. Grandbois, M., et al., *How strong is a covalent bond?* Science, 1999. **283**(5408): p. 1727-1730.

90. Strick, T.R., et al., *The elasticity of a single supercoiled DNA molecule.* Science, 1996. **271**(5257): p. 1835-1837.

91. Strick, T.R., et al., *Behavior of supercoiled DNA.* Biophysical Journal, 1998. **74**(4): p. 2016-2028.

92. Allemand, J.F., et al., *Stretched and overwound DNA forms a Pauling-like structure with exposed bases.* Proceedings of the National Academy of Sciences, 1998. **95**(24): p. 14152-14157.

93. Bryant, Z., et al., *Structural transitions and elasticity from torque measurements on DNA.* Nature, 2003. **424**(6946): p. 338-341.

94. Marko, J.F., *Stretching must twist DNA.* Europhysics Letters, 1997. **38**(3): p. 183.

95. Marko, J.F., *DNA under high tension: Overstretching, undertwisting, and relaxation dynamics.* Physical Review E, 1998. **57**(2): p. 2134-2149.

96. Léger, J.F., et al., *Structural transitions of a twisted and stretched DNA molecule.* Physical Review Letters, 1999. **83**(5): p. 1066-1069.

97. Sarkar, A., et al., *Structural transitions in DNA driven by external force and torque.* Physical Review E, 2001. **63**(5): p. 051903.

98. Bustamante, C., Z. Bryant, and S.B. Smith, *Ten years of tension: single-molecule DNA mechanics.* Nature, 2003. **421**(6921): p. 423-427.

99. Strick, T., et al., *Twisting and stretching single DNA molecules.* Progress in Biophysics and Molecular Biology, 2000. **74**(1–2): p. 115-140.

100. Pauling, L. and R.B. Corey, *A proposed structure for the nucleic acids.* Proceedings of the National Academy of Sciences, 1953. **39**(2): p. 84-97.

101. Gore, J., et al., *DNA overwinds when stretched.* Nature, 2006. **442**(7104): p. 836-839.

102. Rouzina, I. and V.A. Bloomfield, *Force-induced melting of the DNA double helix 1. Thermodynamic analysis.* Biophysical Journal, 2001. **80**(2): p. 882-893.

103. Rouzina, I. and V.A. Bloomfield, *Force-induced melting of the DNA double helix. 2. Effect of solution conditions.* Biophysical Journal, 2001. **80**(2): p. 894-900.

104. Evans, E. and K. Ritchie, *Dynamic strength of molecular adhesion bonds.* Biophysical Journal, 1997. **72**(4): p. 1541-1555.

105. Williams, M.C., et al., *Effect of pH on the overstretching transition of double-stranded DNA: Evidence of force-induced DNA melting.* Biophysical Journal, 2001. **80**(2): p. 874-881.

106. Williams, M.C., et al., *Entropy and heat capacity of DNA melting from temperature dependence of single molecule stretching.* Biophysical Journal, 2001. **80**(4): p. 1932-1939.

107. Cocco, S., et al., *Overstretching and force-driven strand separation of double-helix DNA.* Physical Review E, 2004. **70**(1): p. 011910.

108. Storm, C. and P.C. Nelson, *Theory of high-force DNA stretching and overstretching.* Physical Review E, 2003. **67**(5): p. 051906.

109. Shokri, L., et al., *DNA Overstretching in the presence of glyoxal: Structural evidence of force-induced DNA melting.* Biophysical Journal, 2008. **95**(3): p. 1248-1255.

110. Danilowicz, C., et al., *The structure of DNA overstretched from the 5'5' ends differs from the structure of DNA overstretched from the 3'3' ends.* Proceedings of the National Academy of Sciences, 2009. **106**(32): p. 13196-13201.

111. Albrecht, C.H., et al., *Molecular force balance measurements reveal that double-stranded DNA unbinds under force in rate-dependent pathways.* Biophysical Journal, 2008. **94**(12): p. 4766-4774.

112. van Mameren, J., et al., *Unraveling the structure of DNA during overstretching by using multicolor, single-molecule fluorescence imaging.* Proceedings of the National Academy of Sciences, 2009. **106**(43): p. 18231-18236.

113. Murade, C.U., et al., *Force spectroscopy and fluorescence microscopy of dsDNA-YOYO-1 complexes: implications for the structure of dsDNA in the overstretching region.* Nucleic Acids Research, 2010. **38**(10): p. 3423-3431.

114. Fu, H., et al., *Two distinct overstretched DNA states.* Nucleic Acids Research, 2010. **38**(16): p. 5594-5600.

115. Fu, H., et al., *Transition dynamics and selection of the distinct S-DNA and strand unpeeling modes of double helix overstretching.* Nucleic Acids Research, 2011. **39**(8): p. 3473-3481.

116. Bianco, P., et al., *PicoNewton-millisecond force steps reveal the transition kinetics and mechanism of the double-stranded DNA elongation.* Biophysical Journal, 2011. **101**(4): p. 866-874.

117. Paik, D.H. and T.T. Perkins, *Overstretching DNA at 65 pN does not require peeling from free ends or nicks.* Journal of the American Chemical Society, 2011. **133**(10): p. 3219-3221.

118. Maaloum, M., A.F. Beker, and P. Muller, *Secondary structure of double-stranded DNA under stretching: Elucidation of the stretched form.* Physical Review E, 2011. **83**(3): p. 031903.

119. Kolb, H.C., M.G. Finn, and K.B. Sharpless, *Click chemistry: Diverse chemical function from a few good reactions.* Angewandte Chemie International Edition, 2001. **40**(11): p. 2004-2021.

120. Tornøe, C.W., C. Christensen, and M. Meldal, *Peptidotriazoles on solid phase: [1,2,3]-triazoles by regiospecific copper(I)-catalyzed 1,3-dipolar cycloadditions of terminal alkynes to azides.* The Journal of Organic Chemistry, 2002. **67**(9): p. 3057-3064.

121. Rostovtsev, V.V., et al., *A stepwise Huisgen cycloaddition process: Copper(I)-catalyzed regioselective "ligation" of azides and terminal alkynes.* Angewandte Chemie International Edition, 2002. **41**(14): p. 2596-2599.

122. Meldal, M. and C.W. Tornøe, *Cu-catalyzed azide−alkyne cycloaddition.* Chemical Reviews, 2008. **108**(8): p. 2952-3015.

123. Chan, T.R., et al., *Polytriazoles as copper(I)-stabilizing ligands in catalysis.* Organic Letters, 2004. **6**(17): p. 2853-2855.

124. Kumar, R., et al., *Template-directed oligonucleotide strand ligation, covalent intramolecular DNA circularization and catenation using click chemistry.* Journal of the American Chemical Society, 2007. **129**(21): p. 6859-6864.

125. Lundberg, E.P., et al., *A new fixation strategy for addressable nano-network building blocks.* Chemical Communications, 2010. **46**(21): p. 3714-3716.

126. Lundberg, E.P., et al., *Nanofabrication yields. Hybridization and click-fixation of polycyclic DNA nanoassemblies.* ACS Nano, 2011. **5**(9): p. 7565-7575.

127. El-Sagheer, A.H., et al., *A very stable cyclic DNA miniduplex with just two base pairs.* ChemBioChem, 2008. **9**(1): p. 50-52.

128. Kočalka, P., A.H. El-Sagheer, and T. Brown, *Rapid and efficient DNA strand cross-linking by click chemistry.* ChemBioChem, 2008. **9**(8): p. 1280-1285.

129. Stellwagen, N.C., *Electrophoresis of DNA in agarose gels, polyacrylamide gels and in free solution.* Electrophoresis, 2009. **30**(S1): p. S188-S195.

130. Viovy, J.-L., *Electrophoresis of DNA and other polyelectrolytes: Physical mechanisms.* Reviews of Modern Physics, 2000. **72**(3): p. 813-872.

131. Pavlov, V.M., et al., *Specific fragmentation of T7 phage DNA at low-melting sites.* Nucleic Acids Research, 1977. **4**(11): p. 4053-4062.

132. Lyamichev, V.I., et al., *Localization of low-melting regions in phage T7 DNA.* Nucleic Acids Research, 1983. **11**(7): p. 2165-2176.

133. Lyubchenko, Y.L., et al., *A comparison of experimental and theoretical melting maps for replicative form of φX174 DNA.* Nucleic Acids Research, 1982. **10**(6): p. 1867-1876.

134. Hutton, J.R. and J.G. Wetmur, *Effect of chemical modification on the rate of renaturation of deoxyribonucleic acid. Deaminated and glyoxalated deoxyribonucleic acid.* Biochemistry, 1973. **12**(3): p. 558-563.

135. Broude, N.E. and E.I. Budowsky, *The reaction of glyoxal with nucleic acid components III. Kinetics of the reaction with monomers.* Biochimica et Biophysica Acta (BBA) - Nucleic Acids and Protein Synthesis, 1971. **254**(3): p. 380-388.

136. Broude, N.E. and E.J. Budowsky, *The reaction of glyoxal with nucleic acid components: V. Denaturation of DNA under the action of glyoxal.* Biochimica et Biophysica Acta (BBA) - Nucleic Acids and Protein Synthesis, 1973. **294**(3): p. 378-384.

137. Mossa, A., et al., *Dynamic force spectroscopy of DNA hairpins: I. Force kinetics and free energy landscapes.* Journal of Statistical Mechanics: Theory and Experiment, 2009. **2009**(02): p. P02060.

138. Forns, N., et al., *Improving signal/noise resolution in single-molecule experiments using molecular constructs with short handles.* Biophysical Journal, 2011. **100**(7): p. 1765-1774.

139. Liphardt, J., et al., *Reversible unfolding of single RNA molecules by mechanical force.* Science, 2001. **292**(5517): p. 733-737.

140. Elms, Phillip J., et al., *Limitations of constant-force-feedback experiments.* Biophysical Journal, 2012. **103**(7): p. 1490-1499.

141. Morfill, J., et al., *B-S transition in short oligonucleotides.* Biophysical Journal, 2007. **93**(7): p. 2400-2409.

142. Tomac, S., et al., *Ionic effects on the stability and conformation of peptide nucleic acid complexes.* Journal of the American Chemical Society, 1996. **118**(24): p. 5544-5552.

143. Zhang, X., et al., *Revealing the competition between peeled ssDNA, melting bubbles, and S-DNA during DNA overstretching by single-molecule calorimetry.* Proceedings of the National Academy of Sciences, 2013. **110**(10): p. 3865-3870.

144. King, G.A., et al., *Revealing the competition between peeled ssDNA, melting bubbles, and S-DNA during DNA overstretching using fluorescence microscopy.* Proceedings of the National Academy of Sciences, 2013. **110**(10): p. 3859-3864.